Structural Basis for the Binding of Didemnins to Human Elongation Factor eEF1A and Rationale for the Potent Antitumor Activity of These Marine Natural Products

Esther Marco,[†] Sonsoles Martín-Santamaría,[†,‡] Carmen Cuevas,[§] and Federico Gago*[,†]

Departamento de Farmacología, Universidad de Alcalá, E-28871 Alcalá de Henares, Madrid, Spain, and Pharma Mar S.A., Avda. de los Reyes, 1 Polígono Industrial La Mina, E-28770 Colmenar Viejo, Madrid, Spain

Received December 24, 2003

Didemnins and tamandarins are closely related marine natural products with potent inhibitory effects on protein synthesis and cell viability. On the basis of available biochemical and structural evidence and results from molecular dynamics simulations, a model is proposed that accounts for the strong and selective binding of these compounds to human elongation factor eEF1A in the presence of GTP. We suggest that the *p*-methoxyphenyl ring of these cyclic depsipeptides is inserted into the same pocket in eEF1A that normally lodges either the 3′ terminal adenine of aminoacylated tRNA, as inferred from two prokaryotic EF-Tu·GTP·tRNA complexes, or the aromatic side chain of Phe/Tyr-163 from the nucleotide exchange factor eEF1Bα, as observed in several X-ray crystal structures of a yeast eEF1A:eEF1Bα complex. This pocket, which has a strong hydrophobic character, is formed by two protruding loops on the surface of eEF1A domain 2. Further stabilization of the bound depsipeptide is brought about by additional crucial interactions involving eEF1A domain 1 in such a way that the molecule fits snugly at the interface between these two domains. In the GDP-bound form of eEF1A, this binding site exists only as two separate halves, which accounts for the much greater affinity of didemnins for the GTP-bound form of this elongation factor. This binding mode is entirely different from those seen in the complexes of the homologous prokaryotic EF-Tu with kirromycin-type antibiotics or the cyclic thiazolyl peptide antibiotic GE2270A. Interestingly, the set of interactions used by didemnins to bind to eEF1A is also distinct from that used by eEF1Bα or eEF1B*β*, thus establishing a competition for binding to a common site that goes beyond simple molecular mimicry. The model presented here is consistent with both available biochemical evidence and known structure−activity relationships for these two classes of natural compounds and synthetic analogues and provides fertile ground for future research.

Introduction

Didemnins and tamandarins (Figure 1) are representatives of a class of cyclic depsipeptides, produced by different ascidians of the family *Didemnidae*, that are endowed with potent inhibitory effects on viral proliferation, immune response, and tumor cell growth. Several excellent reviews have recently covered the discovery, isolation, structure elucidation, synthesis, conformational studies, and structure−activity relationships (SAR) of these interesting molecules that are being used as probes of cell biology.[1,2] Of all the congeners synthesized to date, didemnin B (DB) is probably the best characterized at both the biochemical and cellular levels and will be used here as the prototype of the group. DB has been described as a very rapid apoptosis inducer,[3] and its potent inhibitory effects on protein biosynthesis and cell death were early reported not to be reversed after leaving the cells in contact with this compound for 2 h.[4] The sensitivity of cells to DB increases as they progress into the G1 and S phases and is the least during mitosis.[5] Nevertheless, since it kills cells in all phases of the cell cycle, DB is not considered a phase-specific cytotoxic agent.

When a streptavidin−agarose column preincubated with *N*-biotinylbis(*ϵ*-aminocaproyl)didemnin A (DA) was used to purify putative cellular targets for DB, the major retained protein from a bovine brain lysate was the 49 kDa guanine nucleotide-binding eukaryotic elongation factor eEF1A (formerly called EF-1α).[6] A different affinity column made of aminocaproic acid-tethered DA directly coupled to Affi-Gel-10 was later used for the same purpose, but the majority of eEF1A (isoelectric point of 8.9−9.5) was previously removed from the lysate by using cation exchange chromatography at pH 7.1. In this experiment, binding of residual eEF1A to the column was still evident, but in addition, the lysosomal protein palmitoyl thioesterase 1 (PPT-1) was identified as a secondary binding partner for DB.[7] Binding of DA and DB to PPT-1, however, was shown to depend on the presence of substrate palmitoyl-CoA, and DB-mediated inhibition of this enzyme was characterized as being uncompetitive, which questions its possible in vivo relevance for the antiproliferative effects of DB.[8]

* To whom correspondence should be addressed. Telephone: +34-918 854 514. Fax: +34-918 854 591. E-mail: federico.gago@uah.es.
[†] Universidad de Alcalá.
[‡] Current address: Departamentos de Química Orgánica y Farmacéutica, Facultad de Ciencias Experimentales y de la Salud, Universidad San Pablo CEU, Urbanización Montepríncipe, E-28668 Boadilla del Monte, Madrid, Spain.
[§] Pharma Mar S.A.

10.1021/jm0306428 CCC: $27.50
Published on Web 07/22/2004

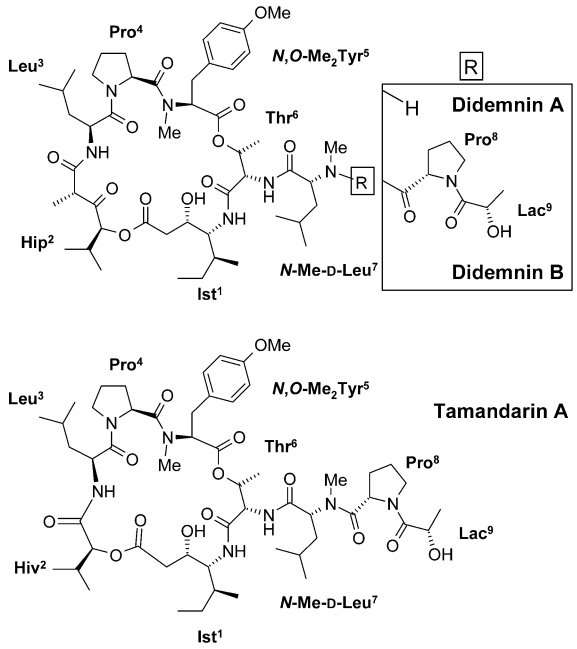

Figure 1. Chemical structures of didemnin A, didemnin B, and tamandarin A. In tamandarins, the 2-(α-hydroxyisovaleryl)propionyl (Hip[2]) residue of didemnins is replaced by an α-hydroxyvaleric acid (Hiv[2]). Numbering follows the usual convention originally assigned to didemnins.[79]

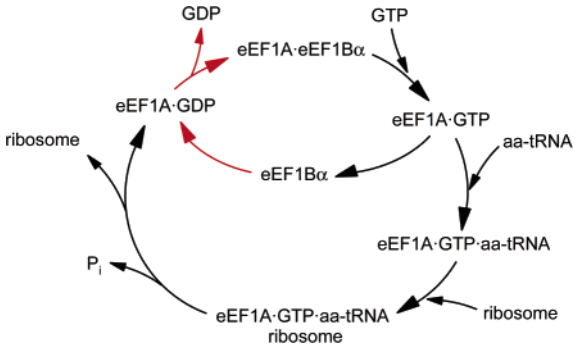

Figure 2. Schematic diagram (modified from ref 27) showing the role of eEF1A and eEF1B (red arrows) in translation elongation. Binding of GTP to eEF1A activates this elongation factor through a conformational change and triggers recruitment of aa-tRNA. The resulting ternary complex then binds to the A-site of the ribosome, thereby forming the quaternary complex depicted at the bottom. Following correct codon−anticodon interaction, GTP is hydrolyzed to GDP, and the resulting inactive eEF1A·GDP complex becomes a target for binding of eEF1B, which then ensures GDP release, thus allowing the reactivation of eEF1A through passive binding of GTP. The translocation of peptidyl-tRNA from the A-site to the P-site is catalyzed by eEF2.

Interestingly, binding of DB to eEF1A was also shown to require the presence of GTP[6,7] even though DB did not block the GTPase activity associated with domain 1 of this G-protein.[6] Consistent with its affinity for eEF1A, DB has been shown to be a potent inhibitor of eukaryotic protein biosynthesis at the elongation stage.[9]

In most eukaryotes, two distinct GTP-dependent elongation factors (eEF1 and eEF2) are required for translation.[10] eEF1 is a pentamer (initially termed $\alpha_2\beta\gamma\delta$, as first described in the brine shrimp *Artemia salina*[11] and each subunit now respectively called eEF1A, eEF1Bα, eEF1Bγ, and eEF1Bβ) that mediates the binding of the cognate aminoacylated tRNA (aa-tRNA) to the A-site of the ribosome and its subsequent release (Figure 2), whereas eEF2 is a monomer and catalyzes the translocation of peptidyl-tRNA from the A-site to the P-site. The four subunits have different functions: eEF1A is activated upon GTP binding and forms a ternary complex with aa-tRNA; eEF1Bα and eEF1Bβ catalyze GDP/GTP exchange on eEF1A·GDP to allow regeneration of eEF1A·GTP; eEF1Bγ binds specifically to membranes and tubulins[12] and has recently been shown to have glutathione S-transferase activity.[13] In good accord with this subunit composition in the eEF1 assembly and the known affinity of didemnins for eEF1A, the stoichiometry of DB binding to ribosomes has been calculated to be approximately 2:1.[14] In addition, binding of DB to ribosome·eEF1A complexes has been reported to be considerably stronger than to eEF1A·GTP in solution.[14]

The structure of eEF1A comprises three domains: domain 1 (residues 1−243) contains the GTP/GDP-binding site and has the typical fold for nucleotide-binding proteins with a central β-sheet surrounded by α-helices (A, A*, A′, B, C*, C, D, and F), whereas domain 2 (residues 244−333) and domain 3 (residues 334−441) are six-stranded β-barrels (numbered a2−f2 and a3−f3, respectively). In common with other GTPases, the GTP/GDP-binding site in domain 1 is formed by five loops (G1−G5) connecting the secondary structure elements. Of the amino acids in the loops that are conserved in this superfamily, a threonine residue is invariably present at the connection between the first α-helix (helix A) and the second β-strand (β-strand b) of this nucleotide-binding domain. Since the side chain oxygen of this threonine is coordinated to the Mg^{2+} ion in the GTP-bound conformation but not in the GDP form, this region has been termed "the effector region" or "switch 1".

In comparison with other small GTPases, eEF1A is a G-protein with a low intrinsic GTP hydrolysis rate that is nevertheless greatly stimulated on the ribosome when the cognate codon−anticodon interaction between mRNA and aa-tRNA takes place.[10] In this situation, GDP has to be released without compromising the ability of GTP to bind to the same site. This is accomplished with the aid of eEF1Bα or eEF1Bβ, both of which behave as nucleotide exchange factors (GEF) catalyzing the exchange of eEF1A-bound GDP for GTP (Figure 2). Translocation of the peptidyl tRNA from the A-site to the P-site is then facilitated by eEF2·GTP, which shares with eEF1A·tRNA the same binding site on the ribosome so that binding of these two translation elongation factors is mutually exclusive.

Since it is this eEF2-dependent translocation that is inhibited by DB (in a strictly eEF1A-dependent fashion), it was suggested that DB might act by stabilizing aa-tRNA bound to the ribosomal A-site.[9] This rather unusual mechanism would then be similar to that of the antibiotic kirromycin, which is known to bind to prokaryotic EF1A (previously termed EF-Tu),[15] even though DB, unlike this antibiotic, does not prevent peptide bond formation. Subsequent experimental results led to the suggestion that eEF2 binding could be prevented by inhibiting eEF1A release from the ribosomal A-site, and two alternative scenarios were then envisaged:[14] (i) direct competition of the DB·eEF1A complex with eEF2 for the same binding site on the

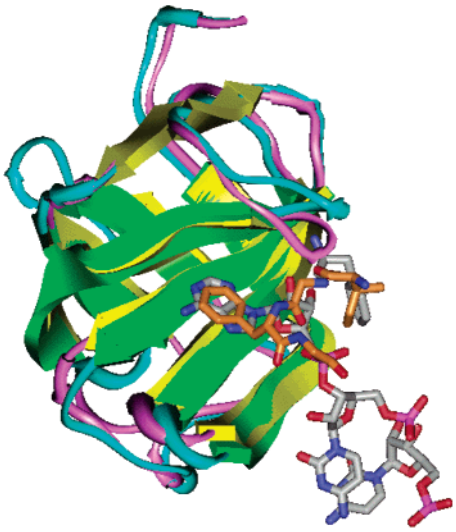

Figure 3. Overlay of domain 2 of *Thermus aquaticus* EF1A (β-sheets in yellow; turns in pink) in its complex (PDB code 1TTT) with GDPNP and Phe-tRNA^{Phe} (C atoms in gray), and domain 2 of yeast eEF1A (β-sheets in green; turns in cyan) in its complex (PDB code 1IJF) with eEF1Bα (C atoms in orange). Ninety-five Cα atoms from each structure were chosen for a least-squares superposition. Note that the 3′ terminal adenine base of tRNA in the former complex and the aromatic side chain of Phe163 in the latter occupy virtually identical positions.

ribosome; (ii) formation of a ribosome·eEF1A·DB complex that would get locked in a conformation that disfavors eEF2 binding, as proposed for ricin. Both of these mechanisms would be consistent with the observation that DB inhibition of translocation can be attenuated by increasing concentrations of eEF2.[9] Thus, although the absolute requirement for eEF1A in DB's action has been conclusively demonstrated, no structural details have been unveiled that could shed light on the way eEF2 binding to pretranslocative ribosome·eEF1A complexes is blocked by this natural product.

Fortunately, available structural information has revealed details about the conformational changes[16,17] undergone by prokaryotic EF1A when it alternates between its active (GTP-bound)[18,19] and inactive (GDP-bound)[20] forms and also about the way EF1A can be recognized by both aa-tRNA[21,22] and the GEF domain of EF1B. In addition, the structures of prokaryotic (formerly termed EF-G)[23] and eukaryotic EF2[24] have also been elucidated, revealing an overall shape similarity ("macromolecular mimicry")[25] between EF2·GDP and EF1A·GTP·tRNA.

Although the basic structures of eEF1A and EF1A have been shown to be very similar[26] and the solution structure of the GEF domain of human eEF1Bα has revealed a striking resemblance to that of EF1B (usually referred to as EF-Ts) from *Escherichia coli*,[27] recognition of eEF1A by eEF1Bα is very different from that observed in the prokaryotic EF1A:EF1B (i.e., EF-Tu:EF-Ts) complex[28] and displays a highly unique feature: one loop of eEF1Bα interacts with domain 2 of eEF1A in the region that is involved in the binding of the CCA-aminoacyl end of tRNA.[21,22] This has been observed in the crystal structure of the complex between eEF1A from *Saccharomyces cerevisiae* and a C-terminal catalytic fragment of eEF1Bα[26] and also in the presence of GDP, GDP and Mg^{2+}, and GDPNP (a nonhydrolyzable analogue of GTP).[29] Interestingly, the conformation that this loop adopts in the crystal structures of these complexes is significantly different from that reported for the equivalent loop in human eEF1Bα previously determined in solution by NMR spectroscopy,[27] which implies mutual adaptation upon complex formation.

When domain 2 of eEF1A in its complex with eEF1Bα is superimposed onto the same region of the GTP-bound form of its bacterial counterpart in complex with Phe-tRNA^{Phe},[21] the terminal adenine base of tRNA and the aromatic side chain of Phe163 from yeast eEF1Bα are found occupying identical positions (Figure 3).[10,29] In this location, between β-strands 258−264 (235−244) and 283−291 (263−271) (where given, numbers in parentheses denote the corresponding residue in *Thermus* EF1A), the side chain of the conserved Glu291(271) stacks on one side of these planar systems whereas the other side sits on the hydrophobic platform made up by the side chain of the conserved Val260(237). When we realized the similarity in shape between the tip of the yeast eEF1Bα hairpin containing Phe163 and the β-turn from which the side chain of *N*,*O*-dimethyltyrosine extends out of the main body of DB (Figure 4), we wondered whether the pocket present on the surface of

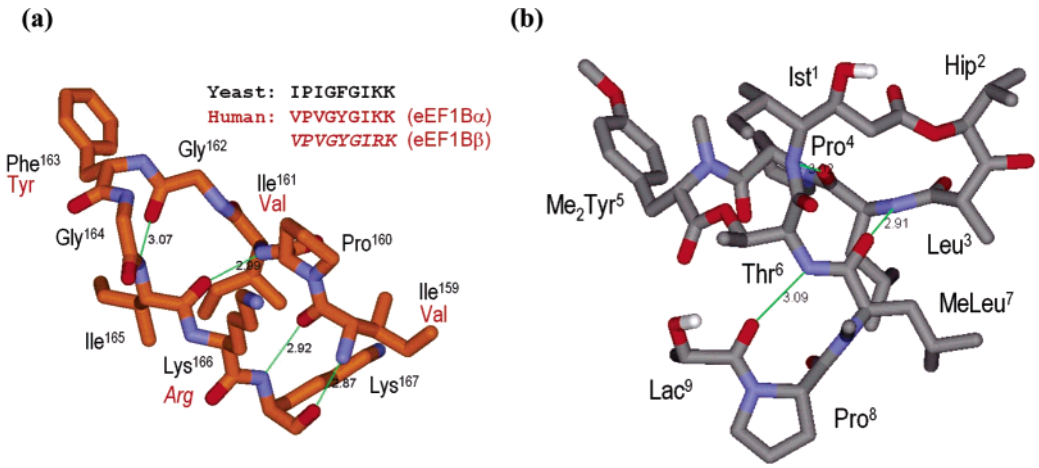

Figure 4. Side-by-side comparison of (a) the tertiary structures of the β2−β3 loop of eEF1Bα containing Phe163 and (b) the X-ray crystal structure of DB.[34] For comparison purposes, the sequences of the yeast eEF1Bα (black) and human eEF1Bα and eEF1Bα (red) hairpins are shown.

```
EF11_HUMAN  MGKEKTHINIVVIGHVDSGKSTTTGHLIYKCGGIDKRTIEKFEKEAAEMGKGSFKYAWVLDKLKAERERGITIDISLWKFETSKYYVTIIDAPGH
EF12_HUMAN  MGKEKTHINIVVIGHVDSGKSTTTGHLIYKCGGIDKRTIEKFEKEAAEMGKGSFKYAWVLDKLKAERERGITIDISLWKFETTKYYITIIDAPGH
EF1A_ARTSA   GKEKIHINIVVIGHVDSGKSTTTGHLIYKCGGIDKRTIEKFEKEAQEMGKGSFKYAWVLDKLKAERERGITIDIALWKFETAKYYVTIIDAPGH
EF1A_YEAST  MGKEKSHINVVVIGHVDSGKSTTTGHLIYKCGGIDKRTIEKFEKEAAELGKGSFKYAWVLDKLKAERERGITIDIALWKFETPKYQVTVIDAPGH
EF11_SCHPO  MGKEKGHINVVVIGHVDSGKSTTTGHLIYKCGGIDKRTIEKFEKEATELGKGSFKYAWVLDKLKAERERGITIDIALWKFETPKYNVTVIDAPGH
EF12_SCHPO  MGKEKGHINVVVIGHVDSGKSTTTGHLIYKCGGIDKRTIEKFEKEATELGKGSFKYAWVLDKLKAERERGITIDIALWKFETPKYNVTVIDAPGH
EFTU_HUMAN  YVRDKPHVNVGTIGHVDHGKTTLTAAITKI--------------LAEGGGAKFKKYEEIDNAPEERARGITINAAHVEYSTAARHYAHTDCPGH
EFTU_THEAQ  FIRTKPHVNVGTIGHVDHGKTTLTAALTYVA-------------AAENPNVEVKDYGDIDKAPEERARGITINTAHVEYETAKRHYSHVDCPGH
EFTU_THETH  FVRTKPHVNVGTIGHVDHGKTTLTAALTYVA-------------AAENPNVEVKDYGDIDKAPEERARGITINTAHVEYETAKRHYSHVDCPGH
              : * *:*: .***** **:* *. :                    :*    ..*    :*:   ** ****: :  ::.*.    :  *.***

EF11_HUMAN  RDFIKNMITGTSQADCAVLIVAAGVGEFEAGISKNGQTREHALLAYTLGVKQLIVGVNKMDSTEPPYSQKRYEEIVKEVSTYIKKIGYNPDTVAF
EF12_HUMAN  RDFIKNMITGTSQADCAVLIVAAGVGEFEAGISKNGQTREHALLAYTLGVKQLIVGVNKMDSTEPAYSEKRYDEIVKEVSAYIKKIGYNPATVPF
EF1A_ARTSA  RDFIKNMITGTSQADCAVLIVAAGVGEFEAGISKNGQTREHALLAYTLGVKQLIVGVNKMDSTEPPFSEARFEEIKKEVSAYIKKIGYNPAAVAF
EF1A_YEAST  RDFIKNMITGTSQADCAILIIAGGVGEFEAGISKDGQTREHALLAFTLGVRQLIVAVNKMDSV--KWDESRFQEIVKETSNFIKKVGYNPKTVPF
EF11_SCHPO  RDFIKNMITGTSQADCAVLIIGGGTGEFEAGISKDGQTREHALLAYTLGVKQLIVAVNKMDTT--GWSQARFEEIVKETSNFIKKVGFNPKTVPF
EF12_SCHPO  RDFIKNMITGTSQADCAILIIGGGTGEFEAGISKDGQTREHALLAYTLGVKQLIVAVNKMDTT--GWSQARFEEIVKETSNFIKKVGFNPKTVPF
EFTU_HUMAN  ADYVKNMITGTAPLDGCILVVAANDGPMP-------QTREHLLLARQIGVEHVVVYVNKADAVQ---DSEMVELVELEIRELLTEFGYKGEETPV
EFTU_THEAQ  ADYIKNMITGAAQMDGAILVVSAADGPMP-------QTREHILLARQVGVPYIVVFMNKVDMVD---DPELLDLVEMEVRDLLNQYEFPGDEVPV
EFTU_THETH  ADYIKNMITGAAQMDGAILVVSAADGPMP-------QTREHILLARQVGVPYIVVFMNKVDMVD---DPELLDLVEMEVRDLLNQYEFPGDEVPV
             *::******::  * .:*::.. * :         ***** ***  :**  ::* :** * .    .    : :  *    :.:  :    ...

EF11_HUMAN  VPISGWNGDNMLEPSANMPWFKGWKVTRKDGNASGTTLLEALDCILP-PTRPTDKPLRLPLQDVYKIGGIGTVPVGRVETGVLKPG---MVVTFA
EF12_HUMAN  VPISGWHGDNMLEPSPNMPWFKGWKVERKEGNASGVSLLEALDTILP-PTRPTDKPLRLPLQDVYKIGGIGTVPVGRVETGILRPG---MVVTFA
EF1A_ARTSA  VPISGWHGDNMLEASDRLPWYKGWNIERKEGKADGKTLLDALDAILP-PSRPTEKPLRLPLQDVYKIGGIGTVPVGRVETGIIKPG---MIVTFA
EF1A_YEAST  VPISGWNGDNMIEATTNAPWYKGWEKETKAGVVKGKTLLEAIDAIEQ-PSRPTDKPLRLPLQDVYKIGGIGTVPVGRVETGVIKPG---MVVTFA
EF11_SCHPO  VPVSGFQGDNMIEPTTNMPWYQGWQKETKAGVVKGKTLLEAIDSIEP-PARPTDKPLRLPLQDVYKIGGIGTVPVGRVETGVIKPG---MIVTFA
EF12_SCHPO  VPVSGFQGDNMIEPTTNMPWYQGWQKETKAGVVKGKTLLEAIDSIEP-PARPTDKPLRLPLQDVYKIGGIGTVPVGRVETGVIKPG---MIVTFA
EFTU_HUMAN  IVGSALCA---LE--GRDP------ELG---LKSVQKLLDAVDTYIPVPARDLEKPFLLPVEAVYSVPGRGTVVTGTLERGILKKGDECELLGHS
EFTU_THEAQ  IRGSALLA---LEEMHKNPKTKRGENEW---VDKIWELLDAIDEYIPTPVRDVDKPFLMPVEDVFTITGRGTVATGRIERGKVKVGDEVEIVGLA
EFTU_THETH  IRGSALLA---LEQMHRNPKTRRGENEW---VDKIWELLDAIDEYIPTPVRDVDKPFLMPVEDVFTITGRGTVATGRIERGKVKVGDEVEIVGLA
            :  *.  .   :*   . *              .   **:*:*     * *  :**: :*:: *:.: * *** .* :* * :: *    ::  :

EF11_HUMAN  PVNVTTEVKSVEMHHEALSEALPGDNVGFNVKNVSVKDVRRGNVAGDSKNDPPMEAAGFTAQVIILNHPGQ---ISAGYAPVLDCHTAHIACKFA
EF12_HUMAN  PVNITTEVKSVEMHHEALSEALPGDNVGFNVKNVSVKDIRRGNVCGDSKSDPPQEAAQFTSQVIILNHPGQ---ISAGYSPVIDCHTAHIACKFA
EF1A_ARTSA  PANITTEVKSVEMHHESLEQASPGDNVGFNVKNVSVKELRRGYVASDSKNNPARGSQDFFAQVIVLNHPGQ---ISNGYTPVLDCHTAHIACKFA
EF1A_YEAST  PAGVTTEVKSVEMHHEQLEQGVPGDNVGFNVKNVSVKEIRRGNVCGDAKNDPPKGCASFNATVIVLNHPGQ---ISAGYSPVLDCHTAHIACRFD
EF11_SCHPO  PAGVTTEVKSVEMHHESLDAGLPGDNVGFNVKNVSVKDIRRGNVCGDSKNDPPMGCASFTAQVIILNHPGQ---ISAGYSPVLDCHTAHIACKFA
EF12_SCHPO  PAGVTTEVKSVEMHHESLDAGLPGDNVGFNVKNVSVKDIRRGNVCGDSKNDPPMGCASFTAQVIILNHPGQ---ISAGYSPVLDCHTAHIACKFA
EFTU_HUMAN  -KNIRTVVTGIEMFHKSLERAEAGDNLGALVRGLKREDLRRGLVMVKPGSIKPHQKVEAQVYILSKEEGGRHKPFVSHFMPVMFSLTWDMACRII
EFTU_THEAQ  PETRKTVVTGVEMHRKTLQEGIAGDNVGLLLRGVSREEVERGQVLAKPGSITPHTKFEASVYILKKEEGGRHTGFFTGYRPQFYFRTTDVTGVVR
EFTU_THETH  PETRRTVVTGVEMHRKTLQEGIAGDNVGVLLRGVSREEVERGQVLAKPGSITPHTKFEASVYVLKKEEGGRHTGFFSGYRPQFYFRTTDVTGVVQ
                 * *..:**.:: *. . .***:*  ::.:. :::.** *  .. .  *         ::  :. *:   : : : * :   * .::  .

EF11_HUMAN  ELKEKIDRRSGKKLEDGPKFLKSGDAAIVDMVPGKPMCVESFSDYPPLGRFAVRDMRQTVAVGVIKAVDKKAAGAGKVTKSAQKAQKAK-
EF12_HUMAN  ELKEKIDRRSGKKLEDNPKSLKSGDAAIVEMVPGKPMCVESFSQYPPLGRFAVRDMRQTVAVGVIKNVEKKSGGAGKVTKSAQKAQKAGK
EF1A_ARTSA  EIKEKCDRRTGKTTEAEPKFIKSGDAAMITLVPSKPLCVEAFSDFPPLGRFAVRDMRQTVAVGVIKSVNFKDPTAGKVTKAAEKAGKKK-
EF1A_YEAST  ELLEKNDRRSGKKLEDHPKFLKSGDAALVKFVPSKPMCVEAFSEYPPLGRFAVRDMRQTVAVGVIKSVDKTEKAA-KVTKAAQKAAKK--
EF11_SCHPO  ELIEKIDRRSGKKIEESPKFVKSGDACIAKMVPSKPMCVEAFTDYAPLGRFAVRDMRQTVAVGVIKAVEKVAPGAAKVTKAAVKAGAKK-
EF12_SCHPO  ELIEKIDRRSGKKIEESPKFVKSGDACIAKMVPSKPMCVEAFTDYAPLGRFAVRDMRQTVAVGVIKAVEKVAPGAAKVTKAAVKAGAKK-
EFTU_HUMAN  LPPEK-------------ELAMPGEDLKFNLILRQPMILEKGQ------RFTLRDGNRTIGTGLVTNTLAMTEEEKNIKWG---------
EFTU_THEAQ  LPQGV-------------EMVMPGDNVTFTVELIKPVALEEGL------RFAIREGGRTVGAGVVTKILE--------------------
EFTU_THETH  LPPGV-------------EMVMPGDNVTFTVELIKPVALEEGL------RFAIREGGRTVGAGVVTKILE--------------------
                            :   .*:     .   :*: :*          **::*:  :*:..*::.
```

Figure 5. Sequence alignment of human eEF1A isoforms 1 (EF11_HUMAN) and 2 (EF12_HUMAN), *Artemia salina* eEF1A (EF1A_ARTSA), *Saccharomyces cerevisiae* eEF1A (EF1A_YEAST, product of genes *TEF1* and *TEF2*), *Schizosaccharomyces pombe* eEF1A isoforms 1 (EF11_SCHPO) and 2 (EF12_SCHPO), human mitochondrial EF1A (EFTU_HUMAN), *Thermus aquaticus* EF1A (EFTU_THEAQ), and *Thermus thermophilus* EF1A (EFTU_THETH). The protein sequences were obtained from Swiss-Prot (http://us.expasy.org/sprot/), and the alignment was produced with the T-Coffee software (http://igs-server.cnrs-mrs.fr/Tcoffee/).[80] Asterisks, colons, and dots designate, respectively, identical or conserved residues in all aligned sequences, conserved substitutions, and semiconserved substitutions. For reference, the strictly conserved threonine involved in coordinating the Mg^{2+} ion and the glutamic acid that stacks onto the terminal adenine of tRNA or Phe163/Tyr162 of eEF1Bα (Thr72/72 and Glu291/293, respectively, in human and yeast eEF1A) are shown in bold.

domain 2 of eEF1A could provide a docking site to this DB's protrusion. Since we were interested in the human protein in its active state, for which no experimental structure is available, we used homology modeling starting from yeast eEF1A followed by steered molecular dynamics (MD) to drive the conformation of domain 1 of eEF1Bα-bound eEF1A into the GTP-bound form for which DB has the strongest affinity. DB was then docked into eEF1A·GTP at the domain 1/2 interface, and finally, the dynamic behavior of the resulting ternary complex was simulated using unrestrained MD.

A working structural model that accounts for DB's potent effects on protein synthesis should explain the differences in affinity between EF1A and eEF1A, the GTP dependence of DB binding to eEF1A, and the molecular basis for preventing binding of eEF2 to the ribosome. The model presented here fulfills all of these requirements and additionally helps to rationalize the SAR for didemnins and related tamandarins, including the increase in bioactivity effected by the modification of DA to DB.

Results

Structural Model of Human eEF1A in the GTP-Bound Conformation. Although the structures of rabbit liver eEF1A·GDP and its complex with tRNA have been analyzed in solution by neutron scattering and microcalorimetric methods,[30] no structure of mammalian eEF1A at the atomic level of detail is currently available. Nevertheless, the highly homologous eEF1A from *Saccharomyces cerevisiae* (Figure 5) has been cocrystallized with a C-terminal catalytic fragment of eEF1Bα, which allows its comparison with both GDP and GTP forms of prokaryotic EF1A and provides a starting structure for modeling the human eEF1A.

Table 1. Cα−Cα Distances (Å) between Residues in Domain 1 That Were Forced To Approach during the Steered Molecular Dynamics (sMD) Simulation of the eEF1A·GTP·Mg^{2+} Complex[a]

	eEF1A:eEF1Bα	DB·eEF1A·GTP·Mg^{2+} [b]	eEF1A·GTP·Mg^{2+} [b]		EF1A·GTP·Mg^{2+}	EF1A·GDP·Mg^{2+}
Leu77 Asp90	7.9	4.7 ± 0.2	4.5 ± 0.1	His67 Asp80	4.6	4.6
Ser76 Ala91	10.1	5.1 ± 0.1	5.1 ± 0.1	Ala66 Cys81	5.2	5.0
Ile75 Pr92	15.3	4.9 ± 0.2	4.9 ± 0.3	Ala65 Pro82	4.7	4.7
Asp74 Gly93	17.4	7.1 ± 0.3	6.8 ± 0.4	Asn64 Gly83	6.7	6.7
Ile73 His94	22.6	7.2 ± 0.3	7.5 ± 0.3	Ile63 His84	8.3	9.1
Ile71 Val16	22.5	6.7 ± 0.4	6.0 ± 0.3	Ile61 Val20	7.9	21.4

[a] For reference, equivalent distances are given for the other complexes mentioned in the text. The distances measured in the EF1A·GTP·Mg^{2+} complex were chosen as part of the target distances that were used for the sMD simulation. [b] Average distance ± standard deviation.

The prokaryotic EF1A·GDP and EF1A·GTP structures show major conformational changes in the effector region. In the former, the C-terminal part of this region is a β-hairpin, whereas in the latter it forms an α-helix.[31] This means that upon GTP binding, Thr62, which is exposed to the solvent in the GDP form (reference distances from OG1 of this residue to magnesium ion are 18.4 and 16.9 Å in EF1A·GDP and eEF1A·GDP:eEF1Bα complexes, respectively), gets involved in the coordination of the Mg^{2+} ion by means of its hydroxyl oxygen because the conserved sequence 60−GITI−63 (Figure 5) comes close to both the phosphate-binding loop (P-loop) and helix B. Another consequence of exchanging GDP with GTP is that the conserved Ile61 gets close to Val20 in the P-loop in such a way that both residues form a "hydrophobic gate" that could be important for GTP hydrolysis.[32]

On the other hand, in both GDP and GTP forms of EF1A, residues Thr65−His67 belong to the second β-strand of domain 1 (β-strand b), whereas in yeast eEF1A the equivalent positions, Ile75−Leu77 (Figure 5), belong to the 70−GITIDIAL−77 loop which is held bound to eEF1Bα by hydrogen bonds. As a result, β-strand b is somewhat shorter as it starts at Trp78, six residues downstream Thr72 in the effector region. In eEF1A, this region is quite different from the equivalent region in EF1A because it comprises two α-helices, A* (Asp35-Gly50) and A′ (Lys55-Arg69), and the Gly70−Leu77 loop, which contains the conserved threonine Thr72 (Figure 5).[19] As regards helix B in the switch 2 region, it extends from Asp97 to Gly105 in the eEF1A:eEF1Bα complex, which means that its location is shifted midway from those found either in the GDP form (His85 to Thr94) or in the GTP form (Ile89 to Ala96) of EF1A.

Given these distinctive characteristics, in our modeling of human eEF1A·GTP from yeast eEF1A:eEF1Bα, it was necessary not only to replace nonidentical amino acids but also to force the initial GDP-bound conformation to reflect the known structural features that have been observed in EF1A·GTP complexes (see Methodology and Table 1). Upon application of the steered MD protocol, domain 1 of human eEF1A conserves the overall topology described for domain 1 of yeast eEF1A but additionally displays the following novel conformational features:

(i) A new hydrophobic cavity lined by Thr38 (from α-helix A*), Leu63 (from α-helix A′), and Trp78 (from β-strand b) is created having a "lid" made up of Asp35 and Arg37 (from α-helix A*).

(ii) β-sheet b is extended relative to the initial structure because it now starts at Ser76, and the loop containing Thr72 is shortened. This 70−GITID−75 loop is maintained close to helix B and the P-loop by a number of hydrophobic and polar contacts similar to those observed in the EF1A·GTP complex. Ile73 (helix B) stacks on Phe98 (loop) (equivalent residues in EF1A are Ile63 and Tyr88), the amino group of Asn101 (helix B) donates a hydrogen bond to the carbonyl oxygen of Ile73 (loop), and the hydrophobic gate described above for the GTP form of EF1A is formed by Val16 (P-loop) and Ile71 (effector region).

(iii) The Mg^{2+} ion coordination sphere is identical with that seen in EF1A·GTP; i.e., it is made up of the hydroxyl oxygen of Thr21 from the P-loop, phosphate oxygens O2γ and O2β from GTP, the hydroxyl oxygen of Thr72 from the effector region, and the oxygens from two water molecules (Table 2).

Table 2. Mean Distances ± Standard Deviation (Å) between Mg^{2+} Cation and Oxygens Involved in Its Coordination Sphere in the DB·EF1A·GTP·Mg^{2+} and EF1A·GTP·Mg^{2+} Complexes[a]

ligand atom	DB·eEF1A·GTP·Mg^{2+}	eEF1A·GTP·Mg^{2+}
Thr72 OG1	2.1 ± 0.3	**3.0 ± 0.3**
Ser21 OG	2.1 ± 0.1	1.9 ± 0.05
GTP O2G	1.8 ± 0.03	1.8 ± 0.02
GTP O2B	1.8 ± 0.03	1.8 ± 0.02
WAT1 O	2.1 ± 0.2	1.9 ± 0.04
WAT2 O	2.1 ± 0.1	**2.7 ± 0.3**

[a] Digits in bold highlight the longer distances in the eEF1A·GTP·Mg^{2+} complex relative to the DB·eEF1A·GTP·Mg^{2+} complex.

Molecular Dynamics of the Human eEF1A·GTP·Mg^{2+} Complex. The resulting model of human eEF1A was simulated using unrestrained MD. After the equilibration period, the progression of the root-mean-square deviations (rmsd) of the coordinates of the Cα atoms with respect to the initial structure showed a notably stable behavior reflecting that the overall architecture of the protein was preserved for the whole length of the simulation (Figure 6). The relatively small rmsd calculated for the complex with respect to the average structure (below 1.0 Å) and the absence of drifting to higher rmsd values were indicative of adequate sampling during the data collection period and suggested that the simulation was long enough to capture the internal dynamics of the eEF1A·GTP·Mg^{2+} complex. Furthermore, the target inter-Cα distances that were

Table 3. Hydrogen Bonds Involved in Stabilization of the Dimerization Interface between Domains 1 and 2 in DB·eEF1A·GTP·Mg^{2+} and EEF1A·GTP·Mg^{2+} Complexes As Monitored during the Molecular Dynamics Simulations[a]

	DB·eEF1A·GTP·Mg^{2+}		eEF1A·GTP·Mg^{2+}		
interaction	mean distance (Å)	standard deviation	mean distance (Å)	standard deviation	homologous interaction in EF1A·GTP·Mg^{2+}
Arg322 NH2:Asp101 OD1	3.7	0.6	5.7	0.8	Arg300 NH2:Asp91 OD1[b]
Tyr86 OH:Glu296 OE2	2.8	0.1	2.9	0.3	
Arg266 NH2:Gln108 O	2.8	0.1	2.9	0.4	Arg241 NH2:Gln98 O[b]
Arg266 NH2:Asp110 OD1	2.7	0.1	2.7	0.1	Arg241 NE:Asp110 OD1[b]
Arg240 NH2:Asp110 OD2	2.7	0.1	2.7	0.1	Arg215 NH2:Asp110 OD2[b]
Arg240 NH1:Asp110 OD1	2.7	0.1	2.7	0.1	Arg215 NH1:Asp110 OD1[b]
Lys79 NZ:Glu297 OE2	4.0	1.0	2.7	0.1	Lys275 NZ:Glu69 OE2[c]
Gly305 O:His7 ND1	3.0	0.3	4.2	0.5	Gly283 O:His11 ND1[b]
Gly305 O:Asn9 ND1	2.8	0.1	2.7	0.1	Gly283 O:Asn13 ND1[b]
Gln108 NE2:Asn307 OD1	2.8	0.2	2.9	0.3	Gln98 NE2:Glu226 OD1

[a] For comparison purposes, equivalent interactions measured in the X-ray crystal structure EF1A·GTP·Mg^{2+} (PDB code 1eft) are given. [b] Residues conserved among species. [c] Correlated mutation.

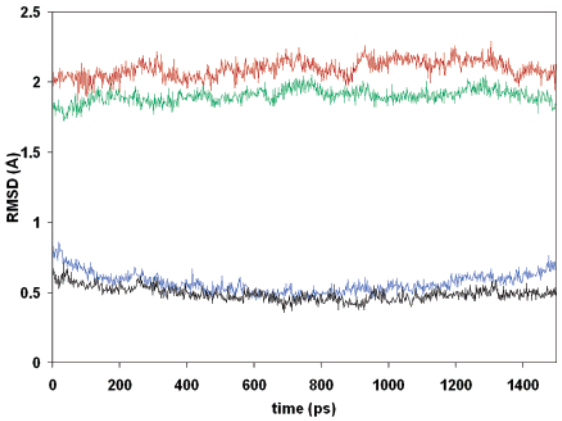

Figure 6. Evolution of the root-mean-square deviations (rmsd) of the Cα atoms of human eEF1A, both in the absence and in the presence of bound DB, with respect to the initial structure (red and green) and the calculated average structure (blue and black). Each line is made up of 750 individual points from the MD trajectory.

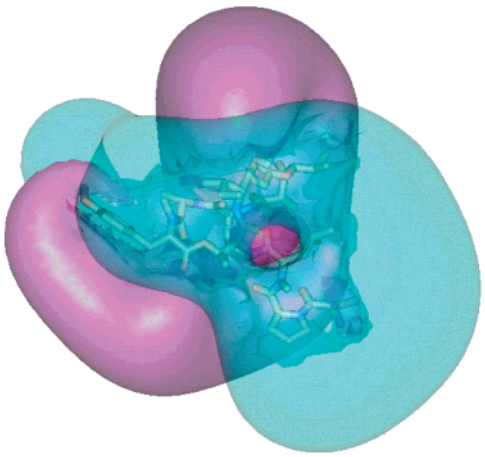

Figure 7. Molecular electrostatic potential of DB (in a conformation similar to that of Figure 4) represented as two semitransparent contours surrounding a stick representation of the molecule (nonpolar hydrogens have been omitted for clarity). Negative (−0.06 to −5.80 kcal mol^{-1}) and positive regions (0.06 to 6.46 kcal mol^{-1}) are colored in pink and blue, respectively.

used during the steered part of the MD simulation (Table 1) were also maintained in the absence of external restraints. The Mg^{2+} ion remained firmly coordinated to four (Thr21, O2γ, O2β, and one water molecule) of the six ligands, whereas the distance between Mg^{2+} and the other water molecule fluctuated between 2.0 and 3.0 Å. Interestingly, the hydroxyl oxygen of Thr72 was kept at even longer distances (Table 2). This loss of full coordination of the magnesium ion could be related in part to the inability of this conformation to effect the hydrolysis of GTP in the absence of the ribosome.

The spatial relationships among the three domains were also maintained during the unrestrained MD simulation. More importantly, the tight interface established between domains 1 and 2, which is stabilized by a number of hydrogen-bonding interactions and salt bridges involving conserved residues (Table 3), determined an extension of the cavity originally present in domain 2 that is known to lodge either the terminal adenine of aa-tRNA or an aromatic residue from the GEF eEF1Bα. This enlarged pocket was then explored computationally as a putative binding site for DB and formed the basis of our subsequent docking studies as described below.

Structural and Electrostatic Characterization of DB. Both NMR[33] and X-ray diffraction[34] studies have shown a highly asymmetric shape for DB, with the macrocycle resembling a twisted figure "8" (Figure 4). The six residues making up the depsipeptide ring structure (isostatine (Ist^1), 2-(α-hydroxyisovaleryl) propionate (Hip^2), leucine (Leu^3), proline (Pro^4), *N*,*O*-dimethyltyrosine (Me_2Tyr^5), and threonine (Thr^6)) have the L configuration, whereas the linear peptide attached to this latter amino acid contains *N*-methyl-D-leucine ($MeLeu^7$) and lactylproline (Pro^8-Lac^9).[2,34] The only transannular hydrogen bond (Ist^1−NH···O=C−Leu^3) that has been described in these experimental structures of DB, as well as in the crystal structure of DA[35] and in the solution structure of dehydrodidemnin B (aplidine),[36] is maintained during the MD simulations in water, as is the Leu^3−NH···O=C−$MeLeu^7$ hydrogen bond that binds the linear chain to the cyclic backbone. In contrast, the hydrogen bond established within the linear part of DB (Thr^6−NH···O=C−Lac^9) is overtly disrupted by competing interactions with water molecules (data not shown). This simulated behavior of DB in aqueous solution highlights the rigidity of the conformationally invariant cyclic depsipeptide and the rather flexible nature of the linear peptide.

Folding of the peptide backbone into a cuplike shape results in a disposition of most of the oxygen atoms of DB pointing away from the interior of the cavity. This particular arrangement gives rise to a molecular elec-

```
EF1B_HUMAN  DDIDLFGSDDEEESEEAKRLREERLAQYESKKAKKPAL-VAKSSILLDVKPWDDETDMAKLEECVRSIQADGLVWGSSKLVPVGYGIKKLQIQCV
EF1D_HUMAN  DDIDLFGSDNEEEDKEAAQLREERLRQYAEKKAKKPAL-VAKSSILLDVKPWDDETDMAQLEACVRSIQLDGLVWGASKLVPVGYGIRKLQIQCV
EF1B_SCHPO  DEIDLFGSD-EEEDPEAERIKAERVAEYNKKKAAKPKA-VHKSLVTLDVKPWDDETPMDELEKAVRSIQMDGLVWGLSKLVPVGFGVNKFQINLV
EF1B_YEAST  DDVDLFGSDDEEADAEAEKWKAERIAAYNAKKAAKPAKPAAKSIVTLDVKPWDDETNLEEMVANVKAIEMEGLTWGAHQFIPIGFGIKKLQINCV
            *::****** ** . ** : : **:  *  *** **   . ** : ********** : ::   *::*: :**.**  :::*:*:*:.*:**: *

EF1B_HUMAN  VEDDKVGTDMLEEQITAFEDYVQSMDVAAFNKI
EF1D_HUMAN  VEDDKVGTDLLEEEITKFEEHVQSVDIAAFNKI
EF1B_SCHPO  VEDDKVSLEALQEELEGFEDYVQSTDIAAMSKL
EF1B_YEAST  VEDDKVSLDDLQQSIEEDEDHVQSTDIAAMQKL
            ******. : *:::.:   *::*** *:**:.*:
```

Figure 8. Sequence alignment of the C-terminal guanine−nucleotide exchange factor domains of human eEF1Bα (EF1B_HUMAN) and eEF1Bβ (EF1D_HUMAN), *Schizosaccharomyces pombe* eEF1B (EF1B_SCHPO), and *Saccharomyces cerevisiae* eEF1B (EF1B_YEAST). The protein sequences were obtained from Swiss-Prot (http://us.expasy.org/sprot/), and the alignment was produced with the T-Coffee software.[80] Shown in bold are the residues that make up the highly homologous loop at whose end the side chain of an aromatic residue (Phe in yeast or Tyr in human) is inserted into domain 2 of eEF1A.

trostatic potential (MEP) for DB that shows the most negative region surrounding one side of the Me_2Tyr^5 side chain, the Ist^1 residue, and one side of the linear peptide moiety and shows the most positive region on the opposite sides of both the Me_2Tyr^5 side chain and the linear part of the molecule (Figure 7). We reasoned that this MEP distribution, together with the hydrophobic effect emanating from the abundant apolar groups present in DB, has to play a major role in the approximation and positioning of the depsipeptide at the target binding site on eEF1A. In fact, the calculated MEP provides a more quantitative description of the previously reported observation that the roughly trigonal array delineated by the Me_2Tyr^5 side chain, the lactylproline moiety, and the hydroxyl group of the Ist^1 residue[34] was likely to define a pharmacophore for interacting with the receptor. The putative binding site for DB on human eEF1A that we have managed to characterize and is described below for the first time provides structure-based support to this early perspicuousness.

Characterization of the DB Binding Site at the Domain 1/2 Interface of Human eEF1A in the GTP-Bound Conformation. The pocket described above encompassing the binding site in domain 2 for the terminal adenine of aa-tRNA or the $\beta2-\beta3$ hairpin aromatic residue from the GEF eEF1Bα extends into the domain 1/2 interface in the GTP conformation of eEF1A. This aromatic residue is Phe163 in yeast but is a tyrosine in both human eEF1Bα and eEF1Bβ (formerly EF-1δ) (Figure 8). This enlarged cavity was further characterized using the CASTp (http://cast.engr.uic.edu/cast/)[37] and GRID (http://www.moldiscovery.com/)[38] programs and was tested as a docking site with the automated docking program AutoDock (http://www.scripps.edu/pub/olson-web/doc/autodock/).

CASTp characterized this interface cavity as the largest one on the protein and calculated values of ∼425 Å^2 and ∼600 Å^3 for its solvent-accessible surface area and volume, respectively. The GRID energy map obtained for the aromatic carbon probe (C1═) highlighted a favorable binding region between the side chains of residues Glu293 and Val262, which form the ceiling and floor, respectively, of the pocket in domain 2 where the aromatic ring of either adenine or Phe163/Tyr162 of eEF1B is known to bind. The hydroxyl probe (O1) predicted favorable interaction sites in the proximity of Asp35 in domain 1 and His296 in domain 2, whereas the sp^3 C probe (C3) highlighted the possibility of van der Waals interactions with the indole ring of Trp78 in

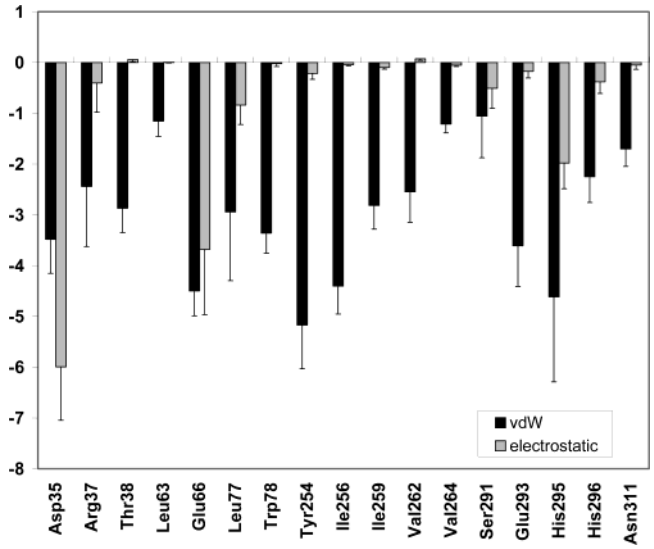

Figure 9. Calculated van der Waals and electrostatic interaction energies (kcal mol^{-1}) between DB and individual eEF1A residues.

β-strand b, Leu63 from helix A′, and Thr38 from helix A*, among others.

AutoDock, on the other hand, produced a limited number of solutions that differed only in the orientation of the flexible linear region. The bulk of the molecule was, in all cases, docked at the interface in an orientation that nicely matched the GRID maps: (i) the Me_2Tyr^5 residue was located in the hydrophobic cavity present in domain 2, in a position similar to that of Phe163 from the eEF1Bα hairpin, that is, in proximity to the side chains of the highly conserved Glu293 and Val262; (ii) the Ist^1 hydroxyl group established favorable interactions with both Asp35 in domain 1 and His296 in domain 2; (iii) the side chain of Hip^2 was placed in the hydrophobic niche created around Trp78, Leu63, and Thr38. The linear peptide attached to Thr^6, on the other hand, showed the largest variation among docked solutions but was invariably placed projecting out of the cavity into the solvent, in good agreement with the fact that this part of the molecule can be attached to an affinity column and still bind eEF1A.[6,7]

Molecular Dynamics and Energy Analysis of the DB·eEF1A·GTP·Mg^{2+} Complex. To assess the feasibility of the proposed binding orientation and to study the mutual adaptation between DB and eEF1A, the DB·eEF1A·GTP·Mg^{2+} complex was refined using energy minimization and its dynamic behavior was simulated using MD; 750 snapshots from the last 1500 ps of the trajectory were then analyzed in terms of intermolecular

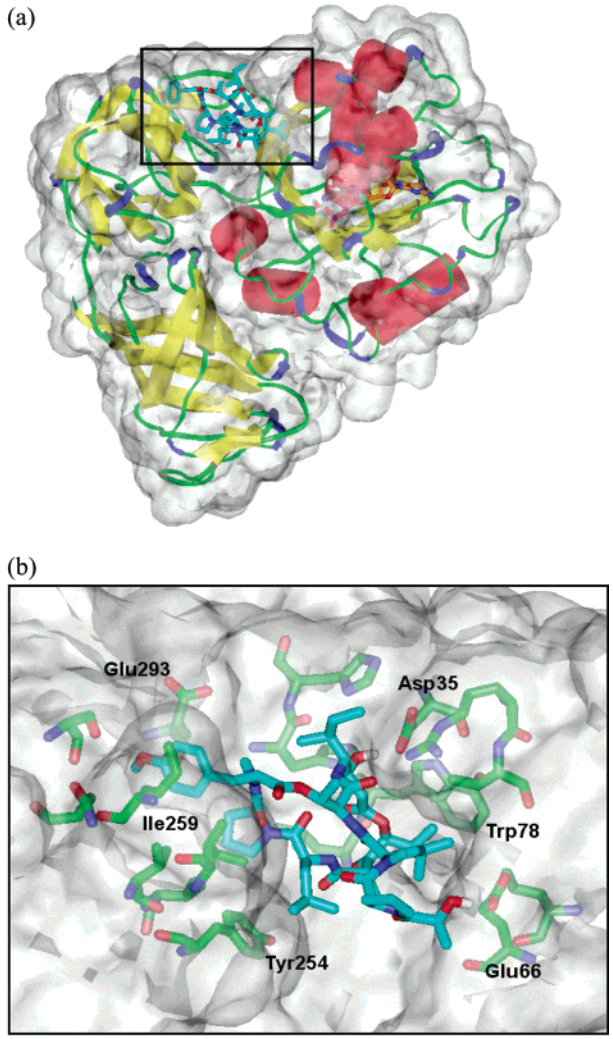

Figure 10. Proposed binding site for DB in human eEF1A1. (a) Schematic representation of the Cα trace of eEF1A1 (α-helices are shown as red barrels, *β*-strands as yellow flat ribbons, and turns as blue arrows), with protein residues enveloped by a semitransparent solvent-accessible surface. Carbon atoms of GTP and DB are colored in orange and cyan, respectively. The Mg^{2+} ion at the catalytic site is shown as a blue sphere, and the two coordinating water molecules are displayed as sticks. (b) Enlarged view of the framed area shown in (a). Some of the protein residues relevant to the discussion have been labeled, and their side chains are shown as sticks. Coordinates for a refined average structure of the DB·eEF1A1·GTP·Mg^{2+} complex have been deposited with the Research Collaboratory for Structural Bioinformatics with identification code RCSB022103 and PDB code 1SYW for immediate release.

energy components (Figure 9) and conformational changes with respect to both the unbound form and a calculated average structure (Figure 10). As seen before for the unbound GTP form of eEF1A, the simulation resulted in a stable trajectory and the relationships among domains, together with the respective interactions, were also maintained, lending further support to the proposed model. The most significant difference observed when DB is bound is that the coordination sphere of the magnesium ion is well preserved and now includes both water molecules and the hydroxyl of Thr72. As a result, the effector domain is slightly displaced (Figure 11) and the geometry of the binding site for the Mg^{2+} ion associated with GTP binding and hydrolysis appears to be optimized when DB is bound relative to the apo form (Table 2).

The energy analysis of the DB·eEF1A·GTP·Mg^{2+} complex (Figure 9) reveals a predominance of van der Waals interactions involving (in decreasing order of magnitude) Tyr254, His295, Glu66, Ile256, Glu293, Asp35, Trp78, Leu77, Thr38, Ile259, Val262, Arg37, His296, Asn311, Val264, Leu63, and Ser291. The electrostatic interactions, on the other hand, appear to be dominated by Asp35, followed by Glu66, His295, and Leu77, all of them engaged in specific hydrogen bonds: the carboxylate of Asp35 as an acceptor for the hydroxyl group of Ist[1], the carboxylate of Glu66 as an acceptor for the hydroxyl group of Lac[9], the imidazole ND1 nitrogen of His295 as a donor to both the carbonyl and hydroxyl oxygens of Ist[1] (i.e., a "bifurcated" hydrogen bond), and the peptide amide of Leu77 as an acceptor for the carbonyl of Hip[2]. This last interaction, which is comparatively smaller in magnitude, is the only one that would be lost in tamandarin A (Figure 1) as a consequence of the replacement of the 2-(α-hydroxyisovaleryl)propionyl residue at position 2 of DB with α-hydroxyvaleric acid (Hiv[2]).

Discussion

It is interesting that the interface between domains 1 and 2 of eEF1A appears to have evolved for the purpose of being broken and specifically reformed, depending on the presence of either GDP or GTP, respectively. The two strikingly different conformations that this elongation factor adopts during its catalytic cycle, depending on the nucleotide bound, have been studied more thoroughly with the bacterial homologue EF1A, also known as EF-Tu.[10]

EF1A is the target of at least two classes of antibiotics that inhibit protein biosynthesis in prokaryotes: the kirromycin family, represented by aurodox, and the cyclic thiazolyl peptide GE2270A. The structures of the complexes between EF1A and each of these antibiotics have been determined by X-ray diffraction techniques. GE2270A makes essentially van der Waals contacts with three segments of amino acids in domain 2 of EF1A·GDP,[39] and one region of the antibiotic binds to the same site as the 3′-end of aa-tRNA. Competition for binding to this site accounts for the effects of the antibiotic on translation inhibition. In contrast, aurodox locks EF1A in its GTP form, even if GDP is bound to the nucleotide-binding site,[15] and prevents binding of EF1B, a GEF formerly known as EF-Ts. However, kirromycin fails to induce the GTP-like conformation of eEF1A·GDP, which explains its inability to inhibit peptide bond formation in the eukaryotic system.[40]

eEF1A binds GDP and GTP in a 1:1 stoichiometry with similar affinity ($K_d' = 2-4\ \mu M$) and, unlike EF1A, can sustain the binding of aa-tRNA to the ribosome also in the presence of GDP or in the absence of any nucleotide, though to a lesser degree than with GTP.[40] Although kirromycin enhances the dissociation rate of the eEF1A·GDP complex, even if not as strongly as eEF1B does, this antibiotic is incapable of increasing the eEF1A·GDP/GTP exchange rate when aa-tRNA and ribosomes are present.

The binding mode we propose for DB on human eEF1A (Figure 10) is entirely different from those

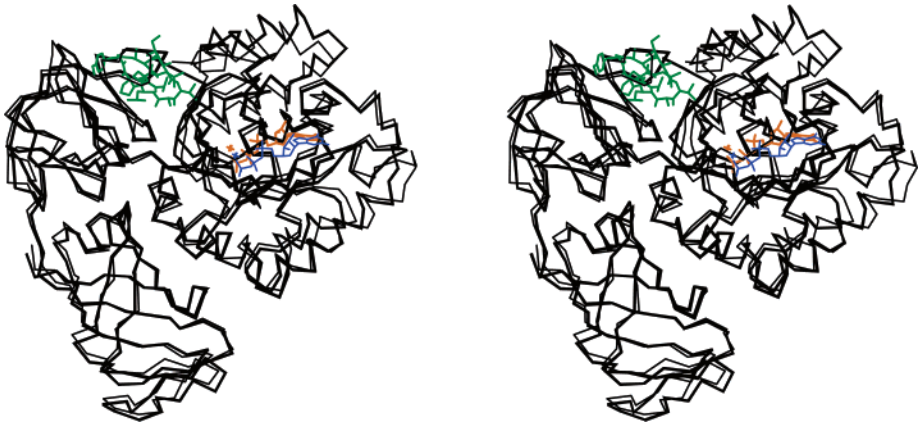

Figure 11. Cα stereotrace of the GTP form of human eEF1A1 in the absence (black thin lines, with GTP in blue) and in the presence of bound DB (black thick lines, with GTP in orange and DB in green). The magnesium ion in the catalytic site of domain 1 is represented as a cross.

observed for either aurodox or GE2270A on prokaryotic EF1A but is reminiscent of the way the loop connecting β-strands 2 and 3 of yeast eEF1Bα binds to yeast eEF1A.[26] The putative binding site for DB is located at the new interface that is created between domains 1 and 2 in the GTP form of eEF1A. The binding interactions involve both hydrophobic and polar contacts, including a number of highly directional hydrogen bonds. Thus, the Ist[1] hydroxyl group donates a hydrogen bond to Asp35 located in helix A* of domain 1, which can nicely explain why acetylation of this hydroxyl group brings about a decreased inhibition of protein biosynthesis[41] and also the importance of the 3*S*,4*R*,5*S* epimer for this residue.[2] At the same time, the carbonyl oxygen of Ist[1] can accept a hydrogen bond from ND1 of His295, located in the loop between β-strands d2 and e2, whereas the methyl that distinguishes DB from nordidemnin B does not participate in the binding, in good accord with the equipotency of these two analogues.[2,42] The carbonyl oxygen of Hip[2] accepts a hydrogen bond from the backbone amide of Leu77 in β-strand b, and the hydrophobic side chain of this same residue is lodged in the cavity formed by the side chains of Trp78, Leu63, and Thr38. It must be emphasized that interaction with these residues is only possible in the GTP conformation in which the conserved GITID loop is close to helix B and the P-loop. If domain 1 of eEF1A, as found in its complex with eEF1Bα, is superimposed onto domain 1 of our modeled DB·eEF1A·GTP·Mg^{2+} complex, a portion of DB occupies the same spatial region that is occupied by these loop residues in the effector region.

The tetrapeptide region of DB (residues 3−6) is primarily in contact with domain 2. The floor and walls of the predominantly hydrophobic pocket in this domain are mostly made up of the side chains of Ile256, Ile259, Val262, and Val264, with the side chain of Glu293 playing the role of a flexible lid. In this cavity, Leu[3] stacks onto Tyr254 (in a similar way to Ile165 of eEF1Bα), Pro[4] is in close van der Waals contact with Val264, and the methoxyphenyl moiety of Me_2-Tyr[5] is inserted between the side chain of Val262 and the methylene group from the side chain of Glu293, establishing additional van der Waals contacts with Ile259 and Ile256. This binding mode satisfactorily accounts for the successful substitution of this dimethylated tyrosine residue with *N*-Me-L-Leu, *N*-Me-L-Phe, or a tetrahydroisoquinoline derivative as well as for the loss of activity that is observed when *N*,*O*-Me_2-Tyr is replaced with the much more hydrophilic *N*-Me-L-Tyr.[2] These findings are in agreement with octanol/water partition coefficient (log $P_{o/w}$) values for benzene derivatives, which reveal a decrease in hydrophobicity of −0.67 log units in going from H to OH compared to just −0.02 when a hydrogen is replaced with a methoxy group.[43] They are, however, apparently in contrast with the fact that Phe or Tyr can occupy the same position at the β2−β3 hairpin of yeast and human eEF1B (Figure 8). In this respect, we note that Phe163 does get sandwiched between the side chains of conserved Glu291 and Val260 in domain 2 of yeast eEF1A, with the carboxylate of the former being hydrogen-bonded to the peptide amide nitrogen.[29] The same is true for the terminal 3′ adenosine in aa-tRNA, which engages its sugar hydroxyl in a hydrogen bond with the equivalent Glu271 of *Thermus* EF1A.[21,22] Thus, in both these experimental structures, the Glu side chain actually stacks on either the phenyl or the adenine ring (Figure 3), whereas in our modeled DB·eEF1A·GTP·Mg^{2+} complex the carboxylate of Glu293 is pointing away from the *p*-methoxyphenyl ring of Me_2-Tyr[5] into the solvent, most likely because of the fact that the equivalent amide nitrogen in DB is methylated. Therefore, we can postulate that the need for a greater hydrophobic character of the Me_2-Tyr[5] residue in DB arises from the lack of this hydrogen-bonding interaction.

The only residue in this tetrapeptide region that contacts with domain 1 is Thr[6] whose carbonyl oxygen accepts a hydrogen bond from the guanidinium group of Arg37 in helix A*. This electrostatic interaction, however, does not appear to be particularly strong (Figure 9), most likely as a result of the positive MEP distribution that surrounds this carbonyl group, as clearly depicted in Figure 7.

MeLeu[7], at the junction of the cyclic and linear parts of DB, interacts with both the side chain methyl of Thr38 and the methylene group from the side chain of Glu66. This binding mode can account for the marked reduction in antitumor activity that was observed upon inversion of the chirality of this residue in nordidemnin,[42] despite a claim that both epimers are equipotent as protein synthesis inhibitors.[2] In the linear part, the role of Pro[8] appears to be only structural whereas the hydroxyl group of Lac[9] establishes a hydrogen bond with the carboxylate of Glu66 in domain

1. This latter interaction implies disruption of the intramolecular hydrogen bond that stabilizes the conventional β-II turn described for both DB in the solid state[34] and dehydrodidemnin B in $CDCl_3$ solution,[36] even though it has been shown to be unnecessary for bioactivity.[2]

This model for DB binding to eEF1A strongly suggests that this natural compound stabilizes the interface between domains 1 and 2 of this elongation factor in the GTP conformation when it is bound to the ribosome just after delivery of the aa-tRNA. In doing so, DB competes with eEF1Bα, thus blocking the crucial guanine nucleotide exchange. As a result, the eEF1A·DB complex remains bound to the ribosomal A-site, thereby preventing binding of eEF2 and the subsequent translocation of peptidyl-tRNA from the A-site to the P-site.

Biological Implications. The reported finding that inhibition of protein synthesis by DB in MCF-7 human breast carcinoma cells occurs at concentrations that are about 1 order of magnitude lower than those required for induction of apoptosis via caspase activation has been taken as evidence for a second mechanism of action and/or a second target protein.[44] PPT-1 has apparently failed to fulfill the role of a secondary pharmacological target,[8] and no obvious structural similarity is apparent between this enzyme[45] and eEF1A beyond the common α/β hydrolase fold. For this reason, it might be worth taking into account that, apart from being an essential partner in the mechanism of translational elongation, eEF1 is considered to be an important multifunctional (moonlighting) protein[46] whose levels are positively correlated with the proliferative state of cells.[47] In animals, eEF1 consists of four different subunits (eEF1A, eEF1Bα, eEF1Bβ, and eEF1Bγ, formerly collectively termed EF-1$\alpha\beta\gamma\delta$) that make up two functionally distinct parts; eEF1A·GTP promotes the binding of aa-tRNA to the A-site of the ribosome under hydrolysis of GTP, whereas the heteromeric complexes eEF1Bα·eEF1Bγ and eEF1Bα·eEF1Bγ·eEF1Bβ function by recycling the resulting inactive eEF1A·GDP intermediate back to the active GTP-bound form by stimulating guanine nucleotide exchange on eEF1A (Figure 2). The highly homologous eEF1Bα and eEF1Bβ (Figure 8) display the same degree of exchange activity[48] but differ with respect to the mode and strength of their interaction with eEF1Bγ.

Among the cellular processes in which eEF1A has been shown to be involved are translational control, cytoskeletal organization, signal transduction, oncogenic transformation, apoptosis, and nuclear processes such as RNA synthesis and mitosis (see refs 49 and 50 for recent reviews). Examples of proteins not directly related to elongation that are known to interact with eEF1A are filamentous actin (F-actin)[51] and the zinc finger protein ZPR1, which is associated with eEF1A and translocated to the nucleus upon treatment of quiescent mammalian cells with mitogens or epidermal growth factor.[52] On the other hand, rapid posttranscriptionally mediated up-regulation of eEF1A has been demonstrated following oxidative stress-induced apoptosis (e.g., upon treatment with hydrogen peroxide).[53] Remarkably, apoptosis induced by dehydrodidemnin has been shown to involve generation of oxidative stress, which can be largely prevented by the glutathione peroxidase mimetic ebselen,[54] and the very weak apoptotic response that is evoked in human normal peripheral blood lymphocytes by this agent (100 nM for 24 h) has been shown to be greatly enhanced in leukemic cells or mitogen-stimulated T-lymphocytes.[55] Since overexpression of eEF1A results in selective resistance to apoptosis induced by growth factor withdrawal and endoplasmic reticulum stress, but not from nuclear damage or death receptor signaling,[56] a global pivotal role of eEF1A levels in the modulation of apoptosis rate has been suggested.[57]

On the other hand, eEF1A has been shown to be overexpressed in metastatic rat mammary adenocarcinoma,[58] and the prostate tumor inducing gene-1 (PTI-1), which is found in human carcinoma cell lines derived from the prostate, lung, breast, and colon, has been shown to encode amino acid residues 65−462 of eEF1A.[50,59] Oncogenic properties have also been attributed to the gene encoding elongation factor eEF1A2,[60] a second isoform (>92% homology) of eEF1A (hereafter termed eEF1A1) that has been found to be amplified in 25% of primary ovarian tumors and to be highly expressed in approximately 30% of ovarian tumors and established cell lines.[61] Another eEF1A isoform has also been identified as the main nuclear protein in human T-lymphoblastic CCRF-CEM cells that specifically recognizes GT oligomers to form a cytotoxicity-related complex that shows a dose-dependent cytotoxic effect on a variety of human cancer cell lines but not on normal human lymphocytes.[62]

This ability of both eEF1A1 and eEF1A2 to form complexes with so many different proteins, which might be explained by the partially unstructured conformation that has been detected in solution for eEF1A,[30] reveals a more complex role for these eEF1 subunits beyond protein biosynthesis. In fact, the multicomponent eEF1 system appears to behave as a sophisticated regulatory factor rather than as a mere "housekeeping" element of the cell, and its activity appears to be coordinated with cell replication. Since many current therapeutic strategies against cancer are directed at DNA or specific protein targets such as enzymes or membrane receptors, the involvement of translational processes and factors in the control of cell proliferation, signal transduction, tumorigenesis, and apoptosis indicates that components of the protein synthesis machinery can be additional targets for anticancer drug design.[63] In this regard, we believe that the actions of didemnins and related agents on these other processes merit further investigation and are consistent with the suggestion that eEF1A may be an appropriate target for novel antitumor or antimetastatic agents.[14]

Conclusions

Inhibition of protein synthesis by DB is known to occur at the elongation stage and to display an absolute requirement for eEF1A, an abundant elongation factor to which it has been shown to bind in a GTP-dependent fashion. The present molecular model helps to rationalize these experimental findings by providing a structural basis for the binding of didemnins and tamandarins to eEF1A and by unraveling some intricacies of this interaction in atomic detail. On the basis of our simulation results, we propose that the binding site for DB

exists only as two separate halves in the GDP-bound form of eEF1A, which accounts for the much greater affinity of DB for the GTP conformation. We show how DB can make use of the extended interface that is formed in the GTP-bound form to stabilize this conformation in a way that does not disrupt GTP hydrolysis. In fact, the eEF1A conformation found in the complex with DB is shown to be fully catalytically competent, unlike the conformation of free eEF1A·GTP, because of a ligand-induced shift of the effector region.

The importance attached to the *p*-methoxyphenyl group of Me_2Tyr^5 of DB as a potential pharmacophoric element, based on the fact that it extends out of the main body of the molecule,[2] has been realized, and the putative hydrophobic nature of the protein pocket where it binds has been confirmed. This pocket, as part of a larger interdomain cavity, is normally used to lodge either the 3′ terminal adenine of aa-tRNA or a crucial aromatic residue from a hairpin of the GEF eEF1Bα, a second elongation factor that is needed for guanine nucleotide exchange upon GTP hydrolysis. Since binding of either eEF1Bα or DB is mutually exclusive, we propose that the rationale behind the potent inhibitory effects on protein synthesis of DB comes as a result of competition with this nucleotide exchange factor.

Taking into account the experimental evidence, DB binding to eEF1A would take place following delivery of aa-tRNA to the ribosome. The resulting DB·eEF1A complex would get stuck at the A-site of the ribosome because binding of the GEF eEF1Bα would be precluded because of occupancy of part of the required site by DB. Stabilization of this complex at the A-site, in turn, would prevent displacement of eEF1A by eEF2 causing translational arrest.[14]

The knowledge gained from this molecular modeling exercise can be applied to elongation factors from other species and, possibly, to other protein−protein interfaces,[64] the stabilization of which might be a goal in the search for novel drugs. We hope that a better understanding of the mechanism of action of DB and related compounds will be beneficial for appropriate use of some of these agents as antiproliferative drugs in a clinical setting. In this regard, the toxicological profile of DB proved to be unfavorable for continuing development,[2] but its close analogue dehydrodidemnin (Aplidin) is presently being evaluated in several phase II clinical trials. The rationale for the unique profile of this potent antitumor agent will be reported elsewhere.

Methodology

Construction and Refinement of Human eEF1A in the GTP-Bound Conformation. The crystal structure of eEF1A in complex with a C-terminal catalytic fragment of eEF1Bα at 1.67 Å resolution (PDB[65] code: 1f60) was used to model the human eEF1A·GTP·Mg^{2+} complex. Yeast and human eEF1A (Figure 5) differ in 80 out of the 440 amino acids that are visible in the electron density map (48 in domain 1, 14 in domain 2, and 18 in domain 3), but none of these are involved in key domain−domain interactions or in binding GTP or the eEF1Bα $\beta2-\beta3$ hairpin. The side chains of nonequivalent residues were replaced in yeast eEF1A with those from its human counterpart using the built-in library of conformers within Insight II.[66] For each "mutated" residue, the rotamer producing the lowest steric clash was chosen. GTP·Mg^{2+}·$(H_2O)_2$ was placed in the nucleotide-binding site in a conformation identical with that found for GDPNP in the X-ray crystal structure of its complex with EF1A (PDB code: 1eft).[18] This starting model was refined using the second-generation AMBER force field[67] and 2000 steps of steepest descent energy minimization while all Cα atoms were restrained to their initial coordinates. This procedure allowed readjustment of covalent bonds and van der Waals contacts without changing the overall conformation of the protein. However, it must be borne in mind that in the GTP conformation domain 1 has to provide additional ligands to stabilize the γ-phosphate and the active site water that will be used as a nucleophile to attack it in the hydrolysis reaction.

To drive the catalytic domain into the "true" GTP conformation, helix B and the preceding loop in the refined starting model (residues 90−109) were manually reoriented to make them adopt the position that they occupy in all known GTP forms of prokaryotic EF1A. Domain 1 was then truncated at residue 238 to immerse the resulting system in a rectangular solvent box extending 8 Å away from any protein atom (∼9000 TIP3P water molecules)[68] for simulating the aqueous environment. Periodic boundary conditions were applied and electrostatic interactions were represented using the smooth particle mesh Ewald method[69] with a grid spacing of ∼1 Å. The coupling constants for the temperature and the pressure baths were 1.0 and 0.2 ps, respectively. Use of the SHAKE algorithm[70] for all bonds involving hydrogens allowed an integration step of 2 fs to be used. The cutoff distance for the nonbonded interactions was 9 Å. The simulation protocol for relaxing this system was essentially as described,[71] involving a series of progressive energy minimizations followed by 200 ps of unrestrained molecular dynamics at 300 K and 1 atm using the SANDER module in AMBER 6.0 (http://amber.scripps.edu/).[72]

The ensuing steered MD (sMD) procedure consisted of pairwise forcing the distances between C_α atoms of residues 77−90, 76−91, 75−92, 74−93, and 73−94 in the original eEF1B-bound form of eEF1A to adopt the same values that are measured between C_α atoms of equivalent residues (67−80, 66−81, 65−82, 64−83, and 63−84) in the crystallographic GTP form of EF1A. This was achieved for each distance in turn (in a zipper-like fashion, starting with 77−90 and ending with 73−94) by means of a harmonic potential with a force constant that was progressively increased (1 kcal mol^{-1} $Å^{-2}$ per run) during five consecutive runs of 20 ps each. The incremental use of this term, as previously reported for other systems,[73,74] tends to avoid biasing the trajectory by overcoming artifactual energy barriers that could deprive the simulation of any physical sense. This same methodology was applied thereafter to the distance between the hydroxyl oxygen of Thr72 and Mg^{2+} ion until coordination was effectively accomplished and then to the distance separating the Cα atoms of Val16 and Ile71 until it reproduced the value observed between equivalent residues in EF1A (Val20−Ile61). Once the desired distances were attained, the whole system was relaxed for 200 ps in the absence of any restraints even though positional constraints (5 kcal mol^{-1} $Å^{-2}$) were used for the Cα atoms of helix B to compensate for the absence of domains 2 and 3.

Upon completion of the refinement of GTP-bound domain 1, the GTP form of EF1A was used as a template to build a suitable spatial relationship between the three domains of human eEF1A. Since domains 2 and 3 of yeast eEF1A superimpose perfectly well onto equivalent domains of *Thermus* EF1A in both GDP and GTP forms and since the residues making up the interface between domains 1 and 2 are highly conserved in both prokaryotic and eukaryotic EF1A, we reasoned it would be safe to assume that the relative orientation of the three domains in the GTP forms of eEF1A and EF1A would be the same. For this reason, a refined average structure of domain 1 from the last 200 ps of the previous sMD simulation was best fitted onto domain 1 of EF1A·GDPNP[18] and the same was done with domains 2 and 3, taking special care that all crucial interdomain hydrogen-bonding interactions and salt bridges involving conserved residues were

maintained. The resulting model was energy-minimized as above.

Model Building and Electrostatic Characterization of DB. The X-ray crystal structure of DB[34] was used in the construction of the initial model. Electrostatic potential-derived charges for the nonstandard residues in DB, as well as for GTP·Mg^{2+}, were obtained with the RESP methodology[75] using a 6-31G* basis set as implemented in the Gaussian 98 program.[76]

Finite difference solutions to the linearized Poisson−Boltzmann equation, as implemented in the DelPhi module of Insight II, were used to calculate MEPs and electrostatic free energies. For MEP calculations on DB and the putative eEF1A binding site, cubic grids with a resolution of 1.0 Å were centered on the molecular systems considered following removal of the explicit water molecules, and the charges were distributed onto the grid points. AMBER charges and radii were used. Solvent-accessible surfaces, calculated with a spherical probe with a radius of 1.4 Å, defined the solute boundaries, and a minimum separation of 10 Å was left between any solute atom and the borders of the box. The potentials at the grid points delimiting the box were calculated analytically by treating each charge atom as a Debye−Hückel sphere. The interior of both the protein and the ligand was considered a low-dielectric medium ($\epsilon = 4$), whereas the surrounding solvent was treated as a high-dielectric medium ($\epsilon = 80$) with an ionic strength of 0.145 M.

Characterization of the Putative Binding Site for DB and Docking Studies. Programs GRID and AutoDock were used in a complementary fashion for docking purposes. For the GRID calculations, a 30 Å × 30 Å × 25 Å lattice of points spaced at 0.5 Å was established at the interface between domains 1 and 2 in order to search for binding sites complementary to the functional groups present in DB. Thus, possible interactions between the putative binding pocket and aromatic carbon (C1═), aliphatic carbon (C3), and hydroxyl oxygen (O1) probes were calculated. The dielectric constants chosen were 4.0 for the macromolecule and 80.0 for the bulk water. The resulting grids were contoured at appropriate energy levels (in kcal mol^{-1}: C1═, −2.5; C3, −2.5; OH, −7.0) and graphically displayed. The geometries of the CCA 3′-end of aa-tRNA and the eEF1Bα hairpin, as found in their crystal complexes with EF1A and eEF1A, respectively (PDB entries 1ttt and 1ijf), were used as positive controls of program performance.

The Lamarckian genetic algorithm[77] implemented in AutoDock 3.0 was used to generate docked conformations of DB within the putative binding site at the interface between domains 1 and 2 by randomly changing the overall orientation of the molecule as well as the torsion angles of the linear peptide region. Default settings were used except for number of runs, population size, and maximum number of energy evaluations, which were fixed at 100, 100, and 250 000, respectively. Rapid intra- and intermolecular energy evaluation of each configuration was achieved by having the receptor's atomic affinity potentials for carbon, oxygen, and hydrogen atoms precalculated in a three-dimensional grid with a spacing of 0.375 Å.

Molecular Dynamics of the Ternary Complexes eEF1A·GTP·Mg^{2+} and DB·eEF1A·GTP·Mg^{2+}. The eEF1A·GTP·Mg^{2+} and DB·eEF1A·GTP·Mg^{2+} complexes were solvated by adding a spherical shell of ∼3000 TIP3P water molecules centered at CG1 of Leu77. The radius of this water shell was 35 Å to ensure the solvation of the interdomain cleft in both complexes. These water molecules were first energy-minimized, and then both waters and all protein residues were allowed to relax. In each case, 1000 steps of steepest descent were followed by 2000 steps of conjugate gradient energy minimization. The final coordinate sets were used as input for the subsequent MD simulations. SHAKE was used for all bonds, and the integration time step was 2 fs. Only the water molecules were free to move for the first 100 ps. For the remaining 2000 ps the whole system was allowed to relax. The list of nonbonded pairs was updated every 25 steps, and coordinates were saved every 2 ps for further analysis.

Analysis of the Molecular Dynamics Trajectories. Three-dimensional structures and trajectories were visually inspected using the computer graphics program InsightII. Root-mean-square (rms) deviations from both the initial structures and the average structures, interatomic distances, and snapshot geometries were obtained using the CARNAL module in AMBER. Intermolecular van der Waals energies for individual residues were calculated with the ANAL module, whereas the solvent-corrected residue-based electrostatic interaction energies were calculated with DelPhi, following the procedure described in detail elsewhere.[78]

Acknowledgment. E.M. is the recipient of a research fellowship from Junta de Comunidades de Castilla-La Mancha. We thank Susana Echepare, Raquel García-Nieto, and Jesús Mendieta for their help at the initial stages of this project. Financial support to F.G. from the National Foundation for Cancer Research is gratefully acknowledged. The University of Alcalá Computing Centre and the CIEMAT (Madrid) are thanked for generous allowances of computer time on their SGI R8000 and R14000 servers.

References

(1) Rinehart, K. L. Antitumor compounds from tunicates. *Med. Res. Rev.* **2000**, *20*, 1−27.
(2) Vera, M. D.; Joullié, M. M. Natural products as probes of cell biology: 20 years of didemnin research. *Med. Res. Rev.* **2002**, *22*, 102−145.
(3) Grubb, D. R.; Wolvetang, E. J.; Lawen, A. Didemnin B induces cell death by apoptosis: the fastest induction of apoptosis ever described. *Biochem. Biophys. Res. Commun.* **1995**, *215*, 1130−1136.
(4) Li, L. H.; Timmins, L. G.; Wallace, T. L.; Krueger, W. C.; Prairie, M. D.; Im, W. B. Mechanism of action of didemnin B, a depsipeptide from the sea. *Cancer Lett.* **1984**, *23*, 279−288.
(5) Crampton, S. L.; Adams, E. G.; Kuentzel, S. L.; Li, L. H.; Badiner, G.; Bhuyan, B. K. Biochemical and cellular effects of didemnins A and B. *Cancer Res.* **1984**, *44*, 1796−1801.
(6) Crews, C. M.; Collins, J. L.; Lane, W. S.; Snapper, M. L.; Schreiber, S. L. GTP-dependent binding of the antiproliferative agent didemnin to elongation factor 1 alpha. *J. Biol. Chem.* **1994**, *269*, 15411−15414.
(7) Crews, C. M.; Lane, W. S.; Schreiber, S. L. Didemnin binds to the protein palmitoyl thioesterase responsible for infantile neuronal ceroid lipofuscinosis. *Proc. Natl. Acad. Sci. U.S.A.* **1996**, *93*, 4316−4319.
(8) Meng, L.; Sin, N.; Crews, C. M. The antiproliferative agent didemnin B uncompetitively inhibits palmitoyl protein thioesterase. *Biochemistry* **1998**, *37*, 10488−10492.
(9) SirDeshpande, B. V.; Toogood, P. L. Mechanism of protein synthesis inhibition by didemnin B in vitro. *Biochemistry* **1995**, *34*, 9177−9184.
(10) Andersen, G. R.; Nissen, P.; Nyborg, J. Elongation factors in protein biosynthesis. *Trends Biochem. Sci.* **2003**, *28*, 434−441.
(11) Janssen, G. M. C.; van Damme, H. T. F.; Kriek, J.; Amons, R.; Möller, W. The subunit structure of elongation factor 1 from *Artemia*. Why two α-chains in this complex? *J. Biol. Chem.* **1994**, *269*, 31410−31417.
(12) Janssen, G. M. C.; Möller, W. Elongation factor 1 beta gamma from Artemia. Purification and properties of its subunits. *Eur. J. Biochem.* **1988**, *171*, 119−129.
(13) Kobayashi, S.; Kidou, S.; Ejiri, S. Detection and characterization of glutathione S-transferase activity in rice EF-1$\beta\beta'\gamma$ and EF-1γ expressed in *Escherichia coli*. *Biochem. Biophys. Res. Commun.* **2001**, *288*, 509−514.
(14) Ahuja, D.; Vera, M. D.; SirDeshpande, B. V.; Morimoto, H.; Williams, P. G.; Joullié, M. M.; Toogood, P. L. Inhibition of protein synthesis by didemnin B: how EF-1α mediates inhibition of translocation. *Biochemistry* **2000**, *39*, 4339−4346.
(15) Vogeley, L.; Palm, G. J.; Mesters, J. R.; Hilgenfeld, R. Conformational change of elongation factor Tu (EF-Tu) induced by antibiotic binding. Crystal structure of the complex between EF-Tu·GDP and aurodox. *J. Biol. Chem.* **2001**, *276*, 17149−17155.
(16) Abel, K.; Yoder, M. D.; Hilgenfeld, R.; Jurnak, F. An α to β conformational switch in EF-Tu. *Structure* **1996**, *4*, 1153−1159.
(17) Clark, B. F.; Nyborg, J. The ternary complex of EF-Tu and its role in protein biosynthesis. *Curr. Opin. Struct. Biol.* **1997**, *7*, 110−116.
(18) Kjeldgaard, M.; Nissen, P.; Thirup, S.; Nyborg, J. The crystal structure of elongation factor EF-Tu from *Thermus aquaticus* in the GTP conformation. *Structure* **1993**, *1*, 35−50.

(19) Berchtold, H.; Reshetnikova, L.; Reiser, C. O.; Schirmer, N. K.; Sprinzl, M.; Hilgenfeld, R. Crystal structure of active elongation factor Tu reveals major domain rearrangements. *Nature (London)* **1993**, *365*, 126−132.
(20) Song, H.; Parsons, M. R.; Rowsell, S.; Leonard, G.; Phillips, S. E. Crystal structure of intact elongation factor EF-Tu from *Escherichia coli* in GDP conformation at 2.05 Å resolution. *J. Mol. Biol.* **1999**, *285*, 1245−1256.
(21) Nissen, P.; Kjeldgaard, M.; Thirup, S.; Polekhina, G.; Reshetnikova, L.; Clark, B. F.; Nyborg, J. Crystal structure of the ternary complex of Phe-tRNA^{Phe}, EF-Tu, and a GTP analog. *Science* **1995**, *270*, 1464−1472.
(22) Nissen, P.; Thirup, S.; Kjeldgaard. M.; Nyborg, J. The crystal structure of Cys-tRNA^{Cys}:EFTu:GDPNP reveals general and specific features in the ternary complex and in tRNA. *Structure* **1999**, *7*, 143−156.
(23) Ævarsson, A.; Brazhnikov, E.; Garber, M.; Zheltonosova, J.; Chirgadze, Y.; al-Karadaghi, S.; Svensson, L. A.; Liljas, A. Three-dimensional structure of the ribosomal translocase: elongation factor G from *Thermus thermophilus*. *EMBO J*. **1994**, *13*, 3669−3677.
(24) Jørgensen, R.; Ortiz, P. A.; Carr-Schmid, A.; Nissen, P.; Kinzy, T. G.; Andersen, G. R. Two crystal structures demonstrate very large conformational changes in the eukaryotic translocase. *Nat. Struct. Biol.* **2003**, *10*, 379−385.
(25) Nissen, P.; Kjeldgaard, M.; Nyborg, J. Macromolecular mimicry. *EMBO J*. **2000**, *19*, 489−495.
(26) Andersen, G. R.; Pedersen, L.; Valente, L.; Chatterjee, I.; Kinzy, T. G.; Kjeldgaard, M.; Nyborg, J. Structural basis for nucleotide exchange and competition with tRNA in the yeast elongation factor complex eEF1A:eEF1Bα. *Mol. Cell* **2000**, *6*, 1261−1266.
(27) Pérez, J. M.; Siegal, G.; Kriek, J.; Hård, K.; Dijk, J.; Canters, G. W.; Möller, W. The solution structure of the guanine nucleotide exchange domain of human elongation factor 1β reveals a striking resemblance to that of EF-Ts from *Escherichia coli*. *Struct. Fold. Des.* **1999**, *7*, 217−226.
(28) Kawashima, T.; Berthet-Colominas, C.; Wulff, M.; Cusack, S.; Leberman, R. The structure of the *Escherichia coli* EF-Tu:EF-Ts complex at 2.5 Å resolution. *Nature (London)* **1996**, *379*, 511−518.
(29) Andersen, G. R.; Valente, L.; Pedersen, L.; Kinzy, T. G.; Nyborg, J. Crystal structures of nucleotide exchange intermediates in the eEF1A-eEF1Balpha complex. *Nat. Struct. Biol.* **2001**, *8*, 531−534.
(30) Budkevich, T. V.; Timchenko, A. A.; Tiktopulo, E. I.; Negrutskii, B. S.; Shalak, V. F.; Petrushenko, Z. M.; Aksenov, V. L.; Willumeit, R.; Kohlbrecher, J.; Serdyuk, I. N.; El'skaya, A. V. Extended conformation of mammalian translation elongation factor 1A in solution. *Biochemistry* **2002**, *41*, 15342−15349.
(31) Polekhina, G.; Thirup, S.; Kjeldgaard, M.; Nissen, P.; Lippmann, C.; Nyborg, J. Helix unwinding in the effector region of elongation factor EF-Tu·GDP. *Structure* **1996**, *4*, 1141−1151.
(32) Berchtold, H.; Reshetnikova, L.; Reiser, C. O.; Schirmer, N. K.; Sprinzl, M.; Hilgenfeld, R. Crystal structure of active elongation factor Tu reveals major domain rearrangements. *Nature (London)* **1993**, *365*, 126−132.
(33) Kessler, H.; Will, M.; Antel, J.; Beck, H.; Sheldrick, G. M. Conformational analysis of didemnins. A multidisciplinary approach by means of x-ray, NMR, molecular dynamics, and molecular mechanics techniques. *Helv. Chim. Acta* **1989**, *72*, 530−555.
(34) Hossain, M. B.; van der Helm, D.; Antel, J.; Sheldrick, G. M.; Sanduja, S. K.; Weinheimer, A. J. Crystal and molecular structure of didemnin B, an antiviral and cytotoxic depsipeptide. *Proc. Natl. Acad. Sci. U.S.A.* **1988**, *85*, 4118−4122.
(35) Mayer, S. C.; Carroll, P. J.; Joullié, M. M. The cyclic depsipeptide backbone of the didemnins. *Acta Crystallogr.; Sect. C: Cryst. Struct. Commun.* **1995**, *51*, 1609−1614.
(36) Cárdenas, F.; Thormann, M.; Feliz, M.; Caba, J.-M.; Lloyd-Williams, P.; Giralt, E. Conformational analysis of dehydrodidemnin B (aplidine) by NMR spectroscopy and molecular mechanics/dynamics calculations. *J. Org. Chem.* **2001**, *66*, 4580−4584.
(37) Liang, J.; Edelsbrunner, H.; Woodward, C. Anatomy of protein pockets and cavities: measurement of binding site geometry and implications for ligand design. *Protein Sci.* **1998**, *7*, 1884−1897.
(38) Goodford, P. A computational procedure for determining energetically favorable binding sites on biologically important macromolecules. *J. Med. Chem.* **1985**, *28*, 849−857.
(39) Heffron, S. E.; Jurnak, F. Structure of an EF-Tu complex with a thiazolyl peptide antibiotic determined at 2.35 Å resolution: atomic basis for GE2270A inhibition of EF-Tu. *Biochemistry* **2000**, *39*, 37−45.
(40) Crechet, J. B.; Parmeggiani, A. Characterization of the elongation factors from calf brain. 2. Functional properties of EF-1 alpha, the action of physiological ligands and kirromycin. *Eur. J. Biochem.* **1986**, *161*, 647−653.
(41) Shen, G. K.; Zukoski, C. F.; Montgomery, D. W. A specific binding site in Nb2 node lymphoma cells mediates the effects of didemnin B, an immunosuppressive cyclic peptide. *Int. J. Immunopharmacol.* **1992**, *14*, 63−73.
(42) Jouin, P.; Poncet, J.; Dufour, M.-N.; Aumelas, A.; Pantaloni, A.; Cros, S.; François, G. Antineoplastic activity of didemnin congeners: nordidemnin and modified chain analogues. *J. Med. Chem.* **1991**, *34*, 486-491.
(43) Hansch, C.; Leo, A. In *Substituent Constants for Correlation Analysis in Chemistry and Biology*; John Wiley: New York, 1979.
(44) Beidler, D. R.; Ahuja, D.; Wicha, M. S.; Toogood, P. L. Inhibition of protein synthesis by didemnin B is not sufficient to induce apoptosis in human mammary carcinoma (MCF7) cells. *Biochem. Pharmacol.* **1999**, *58*, 1067−1074.
(45) Bellizzi, J. J.; Widom, J.; Kemp, C.; Lu, J. Y.; Das, A. K.; Hofmann, S. L.; Clardy, J. The crystal structure of palmitoyl protein thioesterase 1 and the molecular basis of infantile neuronal ceroid lipofuscinosis. *Proc. Natl. Acad. Sci. U.S.A.* **2000**, *97*, 4573−4578.
(46) Ejiri, S. Moonlighting functions of polypeptide elongation factor 1: from actin bundling to zinc finger protein R1-associated nuclear localization. *Biosci. Biotechnol. Biochem.* **2002**, *66*, 1−21.
(47) Talukder, A. H.; Jorgensen, H. F.; Mandal, M.; Mishra, S. K.; Vadlamudi, R. K.; Clark, B. F.; Mendelsohn, J.; Kumar, R. Regulation of elongation factor-1alpha expression by growth factors and anti-receptor blocking antibodies. *J. Biol. Chem.* **2001**, *276*, 5636−5642.
(48) van Damme, H. T. F.; Amons, R.; Karssies, R.; Timmers, C. J.; Janssen, G. M.; Möller, W. Elongation factor 1 beta of artemia: localization of functional sites and homology to elongation factor 1 delta. *Biochim. Biophys. Acta* **1990**, *1050*, 241−247.
(49) Negrutskii, B. S.; El'skaya, A. V. Eukaryotic translation elongation factor 1 alpha: structure, expression, functions, and possible role in aminoacyl-tRNA channeling. *Prog. Nucleic Acid Res. Mol. Biol.* **1998**, *60*, 47−78.
(50) Thornton, S.; Anand, N.; Purcell, D.; Lee, J. Not just for housekeeping: protein initiation and elongation factors in cell growth and tumorigenesis. *J. Mol. Med.* **2003**, *81*, 536−548.
(51) Liu, G.; Tang, J.; Edmonds, B. T.; Murray, J.; Levin, S.; Condeelis, J. F-actin sequesters elongation factor 1alpha from interaction with aminoacyl-tRNA in a pH-dependent reaction. *J. Cell Biol.* **1996**, *135*, 953−963.
(52) Gangwani, L.; Mikrut, M.; Galcheva-Gargova, Z.; Davis, R. J. Interaction of ZPR1 with translation elongation factor-1alpha in proliferating cells. *J. Cell Biol.* **1998**, *143*, 1471−1484.
(53) Chen, E.; Proestou, G.; Bourbeau, D.; Wang, E. Rapid up-regulation of peptide elongation factor EF-1alpha protein levels is an immediate early event during oxidative stress-induced apoptosis. *Exp. Cell Res.* **2000**, *259*, 140−148.
(54) García-Fernández, L. F.; Losada, A.; Alcaide, V.; Alvarez, A. M.; Cuadrado, A.; González, L.; Nakayama, K.; Nakayama, K.; Fernández-Sousa, J. M.; Muñoz, A.; Sánchez-Puelles, J. M. Aplidin induces the mitochondrial apoptotic pathway via oxidative stress-mediated JNK and p38 activation and protein kinase C. *Oncogene* **2002**, *21*, 7533−7544.
(55) Gajate, C.; An, F.; Mollinedo, F. Rapid and selective apoptosis in human leukemic cells induced by aplidine through a Fas/CD95- and mitochondrial-mediated mechanism. *Clin. Cancer Res.* **2003**, *9*, 1535−1545.
(56) Talapatra, S.; Wagner, J. D.; Thompson, C. B. Elongation factor-1 alpha is a selective regulator of growth factor withdrawal and ER stress-induced apoptosis. *Cell Death Differ.* **2002**, *9*, 856−861.
(57) Duttaroy, A.; Bourbeau, D.; Wang, X. L.; Wang, E. Apoptosis rate can be accelerated or decelerated by overexpression or reduction of the level of elongation factor-1 alpha. *Exp. Cell Res.* **1998**, *238*, 168−176.
(58) Edmonds, B. T.; Wyckoff, J.; Yeung, Y. G.; Wang, Y.; Stanley, E. R.; Jones, J.; Segall, J.; Condeelis, J. Elongation factor-1 alpha is an overexpressed actin binding protein in metastatic rat mammary adenocarcinoma. *J. Cell Sci.* **1996**, *109*, 2705−2714.
(59) Shen, R.; Su, Z. Z.; Olsson, C. A.; Fisher, P. B. Identification of the human prostatic carcinoma oncogene PTI-1 by rapid expression cloning and differential RNA display. *Proc. Natl. Acad. Sci. U.S.A.* **1995**, *92*, 6778−6782.
(60) Lee, S.; Ann, D. K.; Wang, E. Cloning of human and mouse brain cDNAs coding for S1, the second member of the mammalian elongation factor-1 alpha gene family: analysis of a possible evolutionary pathway. *Biochem. Biophys. Res. Commun.* **1994**, *203*, 1371−1377.
(61) Anand, N.; Murthy, S.; Amann, G.; Wernick, M.; Porter, L. A.; Cukier, I. H.; Collins, C.; Gray, J. W.; Diebold, J.; Demetrick, D. J.; Lee, J. M. Protein elongation factor EEF1A2 is a putative oncogene in ovarian cancer. *Nat. Genet.* **2002**, *31*, 301−305.

(62) Dapas, B.; Tell, G.; Scaloni, A.; Pines, A.; Ferrara, L.; Quadrifoglio, F.; Scaggiante, B. Identification of different isoforms of eEF1A in the nuclear fraction of human T-lymphoblastic cancer cell line specifically binding to aptameric cytotoxic GT oligomers. *Eur. J. Biochem*. **2003**, *270*, 3251−3262.
(63) Caraglia, M.; Budillon, A.; Vitale, G.; Lupoli, G.; Tagliaferri, P.; Abbruzzese A. Modulation of molecular mechanisms involved in protein synthesis machinery as a new tool for the control of cell proliferation. *Eur. J. Biochem*. **2000**, *267*, 3919−3936.
(64) Toogood, P. L. Inhibition of protein−protein association by small molecules: approaches and progress. *J. Med. Chem*. **2002**, *45*, 1543−1558.
(65) Berman, H. M.; Westbrook, J.; Feng, Z.; Gilliland, G.; Bhat, T. N.; Weissig, H.; Shindyalov, I. N.; Bourne, P. E. The Protein Data Bank. *Nucleic Acids Res*. **2000**, *28*, 235−242.
(66) *Insight II*, version 98.0; Molecular Simulations Inc. (9685 Scranton Road, San Diego, CA 92121-2777), 1998.
(67) Cornell, W. D.; Cieplak, P.; Bayly, C. I.; Gould, I. R.; Merz, K. M.; Ferguson, D. M.; Spellmeyer, D. C.; Fox, T.; Caldwell, J. W.; Kollman, P. A. A second generation force field for the simulation of proteins, nucleic acids, and organic molecules. *J. Am. Chem. Soc*. **1995**, *117*, 5179−5197.
(68) Jorgensen, W. L.; Chandrasekhar, J.; Madura, J. D. Comparison of simple potential functions for simulating liquid water. *J. Chem. Phys*. **1983**, *79*, 926−935.
(69) Darden, T. A.; York, D.; Pedersen, L. G. Particle mesh Ewald: an N*log(N) method for computing Ewald sums. *J. Chem. Phys*. **1993**, *98*, 10089−10092.
(70) Ryckaert, J. P.; Ciccoti, G.; Berendsen, H. J. C. Numerical integration of the Cartesian equations of motion of a system with constraints: molecular dynamics of *n*-alkanes. *J. Comput. Phys*. **1977**, *23*, 327−341.
(71) Marco, E.; García-Nieto, R.; Gago, F. Assessment by molecular dynamics simulations of the structural determinants of DNA-binding specificity for transcription factor Sp1. *J. Mol. Biol*. **2003**, *328*, 9−32.
(72) Case, D. A.; Pearlman, D. A.; Caldwell, J. W.; Cheatham, T. E., III; Ross, W. S.; Simmerling, C. L.; Darden, T. A.; Merz, K. M.; Stanton, R. V.; Cheng, A. L.; Vincent, J. J.; Crowley, M.; Tsui, V.; Radmer, R. J.; Duan, Y.; Pitera, J.; Massova, I.; Seibel, G. L.; Singh, U. C.; Weiner, P. K.; Kollman, P. A. *AMBER 6*; University of California: San Francisco, 1999.
(73) Mendieta, J.; Ramírez, G.; Gago, F. Molecular dynamics simulation of the conformational changes of the glutamate receptor ligand-binding core in the presence of glutamate and kainate. *Proteins* **2001**, *44*, 460−469.
(74) Mendieta, J.; Martín-Santamaría, S.; Priego, E.-M.; Balzarini, J.; Camarasa, M.-J.; Pérez-Pérez, M.-J.; Gago, F. Role of histidine-85 in the catalytic mechanism of thymidine phosphorylase as assessed by targeted molecular dynamics simulations and quantum mechanical calculations. *Biochemistry* **2004**, *43*, 405−414.
(75) Cieplak, P.; Cornell, W. D.; Bayly, C. I.; Kollman, P. A. Application of the multimolecule and multiconformational RESP methodology to biopolymers: charge derivation for DNA, RNA and proteins. *J. Comput. Chem*. **1995**, *16*, 1357−1377.
(76) Frisch, M. J.; Trucks, G. W.; Schlegel, H. B.; Scuseria, G. E.; Robb, M. A.; Cheeseman, J. R.; Zakrzewski, V. G.; Montgomery, J. A., Jr.; Stratmann, R. E.; Burant, J. C.; Dapprich, S.; Millam, J. M.; Daniels, A. D.; Kudin, K. N.; Strain, M. C.; Farkas, O.; Tomasi, J.; Barone, V.; Cossi, M.; Cammi, R.; Mennucci, B.; Pomelli, C.; Adamo, C.; Clifford, S.; Ochterski, J.; Petersson, G. A.; Ayala, P. Y.; Cui, Q.; Morokuma, K.; Malick, D. K.; Rabuck, A. D.; Raghavachari, K.; Foresman, J. B.; Cioslowski, J.; Ortiz, J. V.; Stefanov, B. B.; Liu, G.; Liashenko, A.; Piskorz, P.; Komaromi, I.; Gomperts, R.; Martin, R. L.; Fox, D. J.; Keith, T.; Al-Laham, M. A.; Peng, C. Y.; Nanayakkara, A.; Gonzalez, C.; Challacombe, M.; Gill, P. M. W.; Johnson, B. G.; Chen, W.; Wong, M. W.; Andres, J. L.; Head-Gordon, M.; Replogle, E. S.; Pople, J. A. *Gaussian 98*; Gaussian, Inc.: Pittsburgh, PA, 1998.
(77) Morris, G. M.; Goodsell, D. S.; Halliday, R. S.; Huey, R.; Hart, W. E.; Belew, R. K.; Olson, A. J. Automated docking using a Lamarckian genetic algorithm and an empirical binding free energy function. *J. Comput. Chem*. **1998**, *19*, 1639−1662.
(78) Pérez, C.; Ortiz, A. R.; Pastor, M.; Gago, F. Comparative binding energy analysis of HIV-1 protease inhibitors: incorporation of solvent effects and validation as a powerful tool in receptor-based drug design. *J. Med. Chem*. **1998**, *41*, 836−852.
(79) Sakai, R.; Stroh, J. G.; Sullins, D. W.; Rinehart, K. L. Seven new didemnins from the marine tunicate *Trididemnum solidum*. *J. Am. Chem. Soc*. **1995**, *117*, 3734−3748.
(80) Notredame, C.; Higgins, D. G.; Heringa, J. T-Coffee: A novel method for fast and accurate multiple sequence alignment. *J. Mol. Biol*. **2000**, *302*, 205−217.

JM0306428